How long is a hillslope?

Stuart W.D. Grieve,[1]* **Simon M. Mudd**[1] **and Martin D. Hurst**[2]
[1] School of GeoSciences, University of Edinburgh, Edinburgh, UK
[2] British Geological Survey, Keyworth, Nottingham, UK

*Correspondence to: Stuart W.D. Grieve, School of GeoSciences, University of Edinburgh, Drummond St., Edinburgh EH8 9XP, UK. E-mail: s.grieve@ed.ac.uk

Earth Surface Processes and Landforms

ABSTRACT: Hillslope length is a fundamental attribute of landscapes, intrinsically linked to drainage density, landslide hazard, biogeochemical cycling and hillslope sediment transport. Existing methods to estimate catchment average hillslope lengths include inversion of drainage density or identification of a break in slope–area scaling, where the hillslope domain transitions into the fluvial domain. Here we implement a technique which models flow from point sources on hilltops across pixels in a digital elevation model (DEM), based on flow directions calculated using pixel aspect, until reaching the channel network, defined using recently developed channel extraction algorithms. Through comparisons between these measurement techniques, we show that estimating hillslope length from plots of topographic slope versus drainage area, or by inverting measures of drainage density, systematically underestimates hillslope length. In addition, hillslope lengths estimated by slope–area scaling breaks show large variations between catchments of similar morphology and area. We then use hillslope length–relief structure of landscapes to explore nature of sediment flux operating on a landscape. Distinct topographic forms are predicted for end-member sediment flux laws which constrain sediment transport on hillslopes as being linearly or nonlinearly dependent on hillslope gradient. Because our method extracts hillslope profiles originating from every ridge-top pixel in a DEM, we show that the resulting population of hillslope length–relief measurements can be used to differentiate between linear and nonlinear sediment transport laws in soil mantled landscapes. We find that across a broad range of sites across the continental United States, topography is consistent with a sediment flux law in which transport is nonlinearly proportional to topographic gradient. © 2016 The Authors. Earth Surface Processes and Landforms published by John Wiley & Sons Ltd.

KEYWORDS: sediment flux; topographic analysis; hillslopes; length scales

Introduction

Hillslopes cover a vast majority of the Earth's terrestrial surface and provide most of the sediment supplied to fluvial systems. Geomorphologists have long observed links between the geometric form of hillslopes and processes that transport hillslope material into channels, which are driven by a combination of climate, tectonics and biological activity. Relationships between topographic gradient and sediment transport processes have been demonstrated at scales ranging from individual hillslopes to the scale of continental orogens (Ahnert, 1970; Pinet and Souriau, 1988; Burbank *et al.,* 1996; Montgomery and Brandon, 2002; Gabet *et al.,* 2004; Roering *et al.,* 2007). Biological processes such as animal burrowing and tree throw have been shown to leave a quantifiable topographic signature on hillslopes (Yoo *et al.,* 2005; Gabet and Mudd, 2010; Roering *et al.,* 2010). Hillslopes have also been demonstrated to contain information about a landscape's tectonic history within their morphology (Mudd and Furbish, 2005; Hilley and Arrowsmith, 2008; DiBiase *et al.,* 2012; Hurst *et al.,* 2013a). Thus topographic analysis has the potential to discriminate between different modes of sediment transport (Ahnert, 1970; Braun *et al.,* 2001; Furbish, 2003; Heimsath *et al.,* 2005; Herman and Braun, 2006; Roering, 2008). The high resolution of light detection and ranging (LiDAR) data means we can now resolve meter scale features such as

headwater channels (Tarolli and Dalla Fontana, 2009; Vianello *et al.,* 2009; Tarolli, 2014) and tree-throw mounds (Roering *et al.,* 2010) in addition to resolving channel beds (Smart *et al.,* 2004) and debris fan morphology (Schürch *et al.,* 2011). Therefore, by performing reproducible measurements of the geometry of hillslopes using high resolution topographic data, it is possible to understand and quantify the mechanical (Anderson, 2002; Cohen *et al.,* 2009, 2010), biotic (Yoo *et al.,* 2005; Gabet and Mudd, 2010; Roering *et al.,* 2010; Gabet *et al.,* 2014), chemical (Riebe *et al.,* 2003; Mudd and Furbish, 2004; Burke *et al.,* 2007; Yoo *et al.,* 2007), climatic (Gabet *et al.,* 2004; Riebe *et al.,* 2004; Hales and Roering, 2007; Dixon *et al.,* 2009; Dunne *et al.,* 2010) and tectonic (Hilley and Arrowsmith, 2008; DiBiase *et al.,* 2012; Hurst *et al.,* 2013a) processes which are shaping hillslopes, in addition to constraining the control underlying lithology exerts on the landscape (Korup, 2008; Hurst *et al.,* 2013b).

A fundamental measure of hillslopes is their down-slope length. Hillslope length exerts a primary control on the rate of sediment transport through a catchment, which modulates flows of pollutants, nutrients and water, and in addition influences rates of soil erosion at both the hillslope and catchment scale (Mathier *et al.,* 1989; Dunne *et al.,* 1991; Gabriels, 1999; Liu *et al.,* 2000; Kinnell, 2009; Thompson *et al.,* 2010). Consequently, in a catchment which has short hillslope lengths, the signal of a storm event in the catchment's

headwaters will be transmitted more rapidly to the outlet of the catchment than would be the case in an otherwise similar catchment with longer hillslopes (Dunne et al., 1991).

Work to quantify the rate of sediment accumulation on hillslopes by estimating colluvial hollow filling rates requires accurate constraint on the length of the hillslope upslope of the accumulation zone (Reneau et al., 1989; Reneau and Dietrich, 1991). Hillslope length also acts to constrain debris flow hazard in soil mantled landscapes: a scaling relationship between the area of a landslide scar and the volume of its deposit has been demonstrated (Guzzetti et al., 2009; Klar et al., 2011) and the length of a hillslope exerts a fundamental constraint on the maximum source area of landslides (Hurst et al., 2013c).

Hillslope length is governed by the amount of dissection of a landscape by a channel network, a process governed by a range of factors including climate, erosion rate and hillslope morphology (Chorley, 1957; Abrahams and Ponczynski, 1984; Montgomery and Dietrich, 1989; Rinaldo et al., 1995; Oguchi, 1997; Moglen et al., 1998; Tucker and Bras, 1998; DiBiase et al., 2012) and additionally by the roughness of the topographic surface (Dunne et al., 1991; Thompson et al., 2010). On highly diffuse hillslopes, with little vegetation cover to increase surface roughness, the length of overland flow will be reduced, when contrasted with a hillslope characterized by a large amount of microtopography or vegetation (Dunne et al., 1991; Thompson et al., 2010).

The importance of quantifying hillslope length has been recognized for many decades, but doing so has been a challenge: Horton (1932) commented, 'The exact determination of the average distance which rain must travel overground to reach the stream-channels is impracticable.' Owing to advances in both topographic data resolution and computational power Horton's assertion is no longer true.

A number of methods have been proposed to measure hillslope length. It can be estimated through interpretation of slope–area plots (Roering et al., 2007) and analysis of drainage density data (Tucker et al., 2001; DiBiase et al., 2012) and by modelling flow paths along hillslopes (Tucker et al., 2001; DiBiase et al., 2012; Hurst et al., 2012). An estimate of hillslope length averaged over a landscape can also be approximated through spectral analysis of characteristic length scales found in high resolution topography (Perron et al., 2008), however we do not consider this method, as it yields a single length scale for a landscape, which cannot be readily evaluated against the hillslope and basin scale measurements of other techniques.

Since sediment flux and overland flow are in part governed by hillslope length (Dunne et al., 1991), we reason that characterizing hillslope length as a flow path at the hillslope, rather than catchment scale, should be the most reliable description. We therefore set out to compare the length of flow paths against other previously reported measures of hillslope length and consider the distribution of hillslope length measurements across four field sites in the continental United States.

The rate of hillslope sediment flux is a crucial component in understanding landscape evolution, as it is integral in determining both the geometry of hillslopes (Carson and Kirkby, 1972; Dietrich et al., 2003) and their response to climatic and tectonic forcing (Armstrong, 1980, 1987; Rosenbloom and Anderson, 1994; Arrowsmith et al., 1996; Fernandes and Dietrich, 1997; Roering et al., 2001, 2004; Mudd and Furbish, 2005). Here we demonstrate that our method of measuring hillslope length via flow paths can be used to test two common sediment flux laws, by comparing the hillslope length–relief structure of landscapes with theoretical predictions made by each flux law.

Sediment Flux Laws and their Topographic Predictions

A large number of sediment flux laws (cf. Dietrich et al., 2003) have been proposed to describe sediment flux on hillslopes; within this continuum of laws sediment flux can be described as being linearly dependent on hillslope gradient (Culling, 1960; McKean et al., 1993; Tucker and Slingerland, 1997; Small et al., 1999; Booth et al., 2013); nonlinearly dependent on hillslope gradient (Andrews and Bucknam, 1987; Koons, 1989; Anderson, 1994; Howard, 1997; Roering et al., 1999, 2001; Pelletier and Cline, 2007); dependent on the product of soil thickness and hillslope gradient (sometimes called the depth–slope product; Braun et al., 2001; Furbish and Fagherazzi, 2001; Heimsath et al., 2005; Roering, 2008) or described via the motion of individual sediment particles (Foufoula-Georgiou et al., 2010; Tucker and Bradley, 2010; Furbish and Roering, 2013).

Spatially continuous soil thickness data is not available for our field sites and particle motion based models make a wide range of topographic predictions (Foufoula-Georgiou et al., 2010; Tucker and Bradley, 2010; Furbish and Roering, 2013), as they have no analytical solution, meaning that neither of these groups of flux laws can be falsified using topographic data. However, it is possible to falsify the nonlinear or linear models of sediment flux as these two laws predict distinct relief structures which can be measured using high resolution topographic information. Previous tests of the appropriate sediment flux law for a given landscape typically combine topographic analysis and numerical modelling (Roering et al., 2001; Roering, 2008), topographic analysis and field measurements (Roering et al., 1999; Heimsath et al., 2005), field measurements and numerical modelling (Braun et al., 2001; Herman and Braun, 2006;), or a combination of all three of these techniques (Pelletier et al., 2011). Here we demonstrate a test of flux laws using topography alone.

One approach to examining the topographic outcome of different sediment flux laws is to calculate the predicted relief structure of a landscape. Roering et al. (2007) solved a statement of mass conservation along a one dimensional hillslope for hillslopes obeying a nonlinear flux law of the form (Andrews and Bucknam, 1987; Roering et al., 1999, 2001, 2007):

$$\overline{q}_s = \frac{KS}{1 - (|S|/S_c)^2} \qquad (1)$$

where q_s (in dimensions Length^2 Time^{-1}, dimensions henceforth denoted in square brackets as [L]ength, [M]ass and [T]ime) is a volumetric sediment flux per unit contour length, K [L^2 T^{-1}] is a sediment transport coefficient, S [dimensionless in L/L] is hillslope gradient and S_c [dimensionless] is a critical hillslope gradient; as S approaches S_c, q_s asymptotically progresses towards infinity (Figure 1(a)). Relief, R [L], defined as the elevation difference between the hilltop and the channel can be determined from Equation 1 in the case of steady-state hillslopes, where erosion balances uplift and soil thickness does not change over time (Roering et al., 2007). Here, we employ the steady state definition of Mudd and Furbish (2004), whereby a hillslope which retains a steady form with regard to baselevel (the channel at the toe of the hillslope) is deemed to be in steady state (also known as steady topographic form).

Roering et al. (2007) demonstrated that on hillslopes with steady topographic form, R is a function of the erosion rate E [L T^{-1}], the sediment transport coefficient K and the hillslope length L_H [L] where sediment transport can be described by Equation 1. Furthermore, Roering et al. (2007) found by
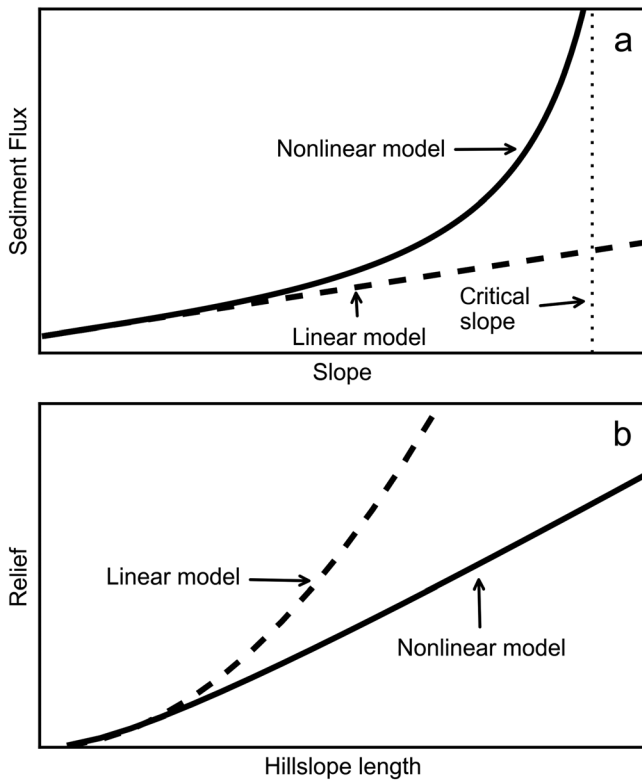
Figure 1. (a) Schematic plot of the relationship between slope and sediment flux for the linear (Equation 1) and nonlinear (Equation 3) flux laws. (b) Schematic plot of the predicted relationship between hillslope length and relief for linear and nonlinear flux laws described by Equations 7 and 8.

normalizing the equation describing hillslope form for these hillslope properties, all steady state hillslopes obeying Equation 1 should fall on a single curve when nondimensional relief $R^* = R/(S_c\ L_H))$ is plotted against nondimensional erosion, $E^* = (-2C_{HT}L_H)/S_c$, where C_{HT} [L^{-1}] is the curvature of the hilltop. Hurst *et al.* (2012) was able to show that in a landscape with a wide range of erosion rates, along the Feather River in northern California, ridgeline-averaged E^* vs R^* data of hilltops fell on the curve predicted by Roering *et al.* (2007), thus providing a test of the nonlinear sediment flux law.

One drawback of this approach is that it requires a distribution of erosion rates in a landscape; Roering *et al.* (2007) tested their theory in landscapes with more spatially homogeneous erosion rates (the Oregon Coast Ranges and Gabilan Mesa, California) and these two landscapes fell upon single points in E^* vs R^* space. Other efforts at constraining flux laws have examined manually selected hillslope profiles (Rosenbloom and Anderson, 1994; Arrowsmith *et al.,* 1996; Furbish and Roering, 2013) or a combination of manually selected hillslope profiles and high resolution topography (Roering *et al.,* 1999). Such profiles are both time consuming to identify and difficult to reproduce without transect coordinates.

Here we use the dimensional relationship between hillslope length, L_H, and relief R, combined with our algorithmic extraction of ridge to valley profiles to examine if topography is more consistent with a particular sediment flux law. One advantage of using dimensional instead of nondimensional length vs relief data is that hillslopes should have a wide range of hillslope lengths so relief and hillslope length may be tested on a large dataset in steadily eroding landscapes. Unlike previous tests of sediment flux laws, this procedure can be performed without field measurements or numerical modelling.

A simple statement of mass conservation on a one-dimensional hillslope, assuming negligible chemical weathering processes, is:

$$\rho_s \frac{\partial z}{\partial t} = -\rho_s \frac{\partial q_s}{\partial x} + \rho_r U, \qquad (2)$$

where z [L] is the elevation of the surface, U [L T^{-1}] is tectonic uplift and ρ_s and ρ_r [M L^{-3}] are soil and rock densities, respectively. At steady state, $U = E$, $\partial z/\partial t = 0$, Equation 2 reduces to $(\rho_r/\rho_s)E = \partial q_s/\partial x$. To close this equation, we must define a sediment flux law, q_s.

One end member sediment flux law is a linear sediment flux law (Figure 1(a)) (Gilbert, 1909; Culling, 1960; Ahnert, 1987):

$$\overline{q}_s = KS \qquad (3)$$

which was first used primarily for its simplicity but has been supported by field studies (McKean *et al.,* 1993; Small *et al.,* 1999) and has been demonstrated to describe sediment transport by rainsplash (Furbish *et al.,* 2007; Dunne *et al.,* 2010). We also consider the nonlinear flux law of Equation 1. We do not consider depth dependent sediment flux because we do not have soil thickness data for all our study sites; thus we cannot truly evaluate all possible flux laws. Rather our goal is to assess whether one of two popular flux laws are consistent with the data and show that, at a minimum, flux laws are falsifiable.

At steady state, the solution of Equation (2) for linear sediment flux is:

$$z(x) = \frac{\rho_r E}{2\rho_s K}\left(x^2 - L_H^2\right) \qquad (4)$$

where the hilltop is located at $x = 0$ and the base of the hillslope is at $x = L_H$. The steady state solution of Equation (2) for nonlinear sediment flux is (Roering *et al.,* 2007):

$$z(x) = \frac{S_c}{\kappa}\left[ln\left(0.5\left[\sqrt{1 + x^2\kappa^2} + 1\right]\right) - \sqrt{1 + x^2\kappa^2} + 1\right] \qquad (5)$$

Where

$$\kappa = \frac{\rho_r E}{2\rho_s K} \qquad (6)$$

The relief is found by subtracting the elevation at the hilltop from the elevation at the hillslope base. In the linear case, relief is:

$$R = \frac{\rho_r\ E}{2\rho_s\ K} L_H^2 \qquad (7)$$

and in the nonlinear case steady state relief is:

$$R = \frac{S_c\left[\sqrt{1 + \kappa^2 L_H^2} + \ln(3) - 1 - \ln\left(2 + \sqrt{1 + \kappa^2 L_H^2}\right)\right]}{\kappa} \qquad (8)$$

Equations (7) and (8) describe contrasting relationships between hillslope length and relief. If sediment transport can be described by a linear flux law, hillslope relief should go as the square of the hillslope length given constant densities, transport coefficients and erosion rates. On the other hand, relief will be approximately linear as a function of hillslope length if sediment flux can be described by a nonlinear sediment flux law of the form in Equation (1) (Figure 1(b)).

In order to test if theoretical predictions of relief as a function of hillslope length are consistent with real topography, we must first ensure that our topographic measurements are consistent

with the assumptions contained within the equations of sediment flux and mass conservation. Equations (7) and (8) are formulated for one-dimensional, soil mantled hillslopes, therefore we must restrict our analysis to hillslope profiles that can be approximated as one-dimensional, and where we can be confident of a persistent soil mantle.

Quasi-one-dimensional hillslope traces are identified by comparing the measured hillslope length to the Euclidean distance between the start and end point of the flow path. If these two values are approximately equal, within a tolerance of 0.02%, we conclude that a trace is planar, and can be described using Equations (7) and (8). In addition, any traces which were initiated on hilltops with a positive hilltop curvature or a slope value of greater than 1.2 are excluded from this analysis, ensuring that hillslopes studied are soil mantled. This filtering can introduce a bias towards shorter hillslopes, as the longer traces have more opportunity to diverge from planarity, and this limitation should be considered when evaluating hillslope length–relief relationships.

Identifying sections of a landscape which approximate one-dimensional hillslope profiles is a key challenge of attempting to test one-dimensional models with topographic data, because significant proportions of upland, soil mantled landscapes are characterized by planform curvature, forcing topographic profiles to deviate from a one-dimensional profile (Roering *et al.,* 1999). Our method generates a large amount of traces for a landscape, and can filter them automatically to find all of the quasi-one-dimensional traces in an area. However, such traces can be rare, limiting the validity of tests of flux laws using this method, particularly where only a small area of a landscape is covered by the filtered topographic data.

Methods

Topographic processing

In order to implement and test techniques for extracting hillslope length from high resolution topography we must ensure consistency in how topographic processing is performed. The topographic derivatives of slope, aspect and curvature are required for all three of the hillslope length extraction techniques. We calculate these derivatives following techniques outlined by Lashermes *et al.* (2007); Roering *et al.* (2010) and Hurst *et al.* (2012) to fit a polynomial surface to elevation values within a circular window, passed across every cell in the DEM. The radius of the circular window is determined by identifying breaks in values of the interquartile range and standard deviation of curvature as a function of window size. This ensures that the slope values are representative of slope at the hillslope scale rather than a function of the combination of microtopographic variations, such as the roughening of hillslopes from tree throw, and measurement noise produced during LiDAR data acquisition (Roering *et al.,* 2010; Hurst *et al.,* 2012).

The foundation of the hilltop flow routing and drainage density inversion methods is being able to define the location of channels. Without an accurate constraint of the location of the channel network neither method will be accurate. Each of these techniques therefore require precise mapping of the location of the channel head, either through field exploration (Julian *et al.,* 2012; Jefferson and McGee, 2013), a process based method (Clubb *et al.,* 2014), geomorphometric analysis of a DEM (Passalacqua *et al.,* 2010; Orlandini *et al.,* 2011; Pelletier, 2013) or contour map (Oguchi, 1997). Here, we extract channels from the DEM following the DrEICH method outlined by Clubb *et al.* (2014), using the parameters in Supplementary

Table 2. In addition, large floodplains were identified in each landscape as patches of low positive local relief and low slope. Local relief was calculated as the range in elevations in a circular moving window, of the same radius as the window used to fit the polynomial surface, passed over the landscape. These patches were then manually combined to create contiguous patches of floodplain. This floodplain mask was then combined with the channel network to include the floodplain extent, ensuring that only the hillslope portion of each landscape is sampled.

Basins are extracted by identifying junctions in the channel network where the Strahler stream order increases and then identifying all of the upslope pixels for that junction. Drainage area is calculated using the D-infinity algorithm (Tarboton, 1997).

Extracting hillslope length using slope–area analysis

Relationships between local slope and drainage area have been used to identify process transitions in landscapes (Montgomery, 2001; Stock and Dietrich, 2003; Roering *et al.,* 2007; Tarolli and Dalla Fontana, 2009; Booth *et al.,* 2013; Tarolli, 2014; *Tseng et al.,* 2015). In areas where hillslope processes dominate, slope increases with drainage area and in areas where fluvial processes dominate slope decreases with increasing drainage area (Montgomery and Foufoula-Georgiou, 1993). Therefore, the transition between the hillslope and fluvial domain can be identified as the first inflection point in slope–area space (Figure 2) (Montgomery and Foufoula-Georgiou, 1993; Hancock and Evans, 2006; Tarolli and Dalla Fontana, 2009). As drainage area increases beyond this transition point, further scaling breaks have been demonstrated to correspond with large-scale landsliding (Tarolli and Dalla Fontana, 2009; Booth *et al.,* 2013; Tarolli, 2014; Tseng *et al.,* 2015).

Slope [dimensionless in L/L] and drainage area [L^2] are sampled on a per pixel basis for each catchment in the landscape and the resulting values are placed in logarithmically spaced bins with a width of 0.1 in base 10 logarithmic space, with area measured in units of m^2. Binned values are then plotted in log–log space and the algorithm searches for the binned point with the maximum slope value. This maximum slope bin is identified as the inflection point and the corresponding drainage area is recorded. We also record the drainage area of the maximum slope of a cubic spline fitted to the binned data following Roering *et al.* (2007). We have found these two methods pro-
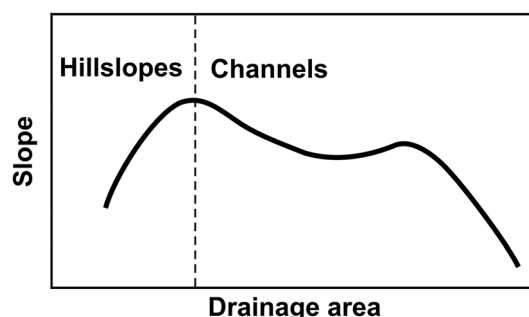

Figure 2. Schematic diagram of a slope–area plot showing the predicted relationship between slope and drainage area in a catchment in a soil mantled landscape. Slope increases with increasing drainage area on hillslopes, while in channels, slope decreases as drainage area increases. The inflection point between these two domains, denoted by the dashed line, is identified as the characteristic drainage area, which is transformed into a representative hillslope length for the particular catchment. The second inflection point corresponds to the signature of large-scale landsliding (Tseng *et al.,* 2015).

duce indistinguishable results and thus results presented in figures use maximum binned slope values as this is less computationally expensive. The resulting characteristic drainage area, often used to identify the threshold area for channel initiation (Montgomery and Dietrich, 1992; Montgomery and Foufoula-Georgiou, 1993) is then converted into a characteristic hillslope length by dividing the area by the unit contour width (Roering *et al.*, 2007), which can be approximated as the DEM resolution (Montgomery and Dietrich, 1989; Moore *et al.*, 1991; Costa-Cabral and Burges, 1994; Mitasova *et al.*, 1996; Tarboton, 1997).

Inversion of drainage density to extract hillslope length

Drainage density (D_D [L]) is a fundamental landscape parameter which has been shown to vary with climate (Chorley, 1957; Abrahams and Ponczynski, 1984; Rinaldo *et al.*, 1995; Moglen *et al.*, 1998), relief (Schumm, 1956; Oguchi, 1997) and dominant sediment transport process (Montgomery and Dietrich, 1989; Willgoose *et al.*, 1991; Tucker and Bras, 1998). It is defined as the total length of the channel network (L_T [L]) divided by the catchment area (A [L^2]) (Horton, 1932, 1945):

$$D_D = \frac{L_T}{A} \quad (9)$$

The drainage density of a catchment provides a measure of the level of dissection of a landscape, the inverse of which will reflect the catchment average hillslope length. This parameter is described by Horton (1932, 1945) and Tucker *et al.* (2001) as the mean distance water must travel from a random point in a catchment to reach a channel and is considered by Schumm (1956) to be equivalent to the catchment average length of overland flow.

This measurement can be quantified as (Horton, 1932; Schumm, 1956; Tucker *et al.*, 2001):

$$L_H \approx (2D_D)^{-1} \quad (10)$$

where L_H [L] is hillslope length; thus drainage density can be transformed into a measurement of the average flow path length of hillslopes in the catchment.

Using hilltop flow routing to measure hillslope length

Building on the work of Hurst *et al.* (2012), we have, in addition, developed a measure of hillslope length in which hillslope length is defined as the typical travel distance from divide to channel (Roering *et al.*, 2007). The simplest method employed to model flow paths is the D8 algorithm, which distributes flow at 45° azimuth angles into the eight neighboring grid cells (Mark, 1984; O'Callaghan and Mark, 1984; Tarboton *et al.*, 1991). This technique operates well when constraining channelized flow (Shelef and Hilley, 2013) and is a commonly used method for extracting a channel network from a DEM (Braun and Willett, 2013). However, when using this algorithm in the hillslope domain, the direct flow paths do not reflect the dispersive nature of overland flow (Tarboton, 1997; Pelletier, 2010; Shelef and Hilley, 2013) and as such the resulting measured hillslope lengths are biased towards short hillslopes. Hurst *et al.* (2012) modified this approach and modelled flow from hilltop to channel as a point source crossing each DEM cell.

Hilltops are extracted by identifying the edges of basins which share a stream order following techniques outlined by Hurst *et al.* (2012). From each of these selected hilltop pixels a trace can be run to measure its flow path to the channel.

We then modify the algorithm of Lea (1992) to model the flow of a point source of water from the ridge line down to the channel. Flow is modelled within each DEM cell, flowing from an inlet point on each cell edge to an outlet point on another cell edge, with the flow path within each cell following that cell's aspect angle. Flow is then routed across each cell from the inlet point (or cell center for hilltop pixels where tracing begins) across to its outlet point. This in-pixel routing is repeated recursively, with the flow outlet becoming the subsequent new inlet as the routing proceeds, until the trace has reached a channel or floodplain pixel. If two cells flow into each other the algorithm calculates the secondary aspect of these two pixels and flow is pushed along the cell edge which corresponds to this secondary aspect until it enters another cell whereby flow can continue.

When using aspect angle calculated from a polynomial fit, areas of high topographic noise can generate large sinks in the topography, where flow cannot be routed to the channel. These large areas commonly correspond to low gradient areas of a landscape, such as terraces, valley fills or areas filled by DEM pre-processing to remove pits. It is not possible to allow flow to pass across these zones without extensive smoothing of the landscape or the trace paths themselves, which will destroy any topographic signal which could otherwise be measured. Therefore these traces, which account for <5% of the total number of traces in the nosiest landscapes and <0.5% in smoother landscapes are excluded from all final analysis.

The initial starting point of the trace is given by Lea (1992) as the cell center for computational simplicity. In high resolution topographic data this placement has little influence on the final results as hillslope length is effectively sampled at intervals along each ridgeline equal to the data resolution.

When our routing algorithm is used to measure hillslope length we are implicitly choosing to quantify sediment transport over millenial timescales, because the calculation of aspect averages the land surface over several cycles of geomorphic roughening (i.e. tree-throw pits are considered transient and do not affect millennial scale sediment transport directions). Our objective for this study is to compare hillslope lengths with predictions of geomorphic flux laws operating over millenial time scales (i.e. the time required to change the relief of the hillslope, sensu Mudd and Furbish, 2007) rather than event-based routing of water, so we route flow over topography which is effectively smoothed using an aspect driven routing technique.

The hilltop flow routing algorithm records a small number of basins with short average hillslope lengths, which is consistent with the typical implementation of the algorithm which will measure hillslope lengths near the basin outlet, where the hillslope length approaches the effective channel width. In some basins the only hilltops that are sampled are these interfluves, due to the filtering of hilltops outlined in this section, to ensure that hillslopes sampled are soil mantled. These values are valid measurements; however their bias in smaller basins requires careful analysis of basin average results and motivates the use of median and median absolute deviation values to minimize the influence of these exceptional measurements on the dataset.

Our flow tracing method not only can be used to measure hillslope length, but it can also be used to measure local relief at the hillslope scale, by calculating the difference in elevation between the start and end point of each trace. We use data collected for hillslope length measurements to explore the relationships between hillslope length and relief at the hillslope scale.

Study Sites

We selected four locations in the continental United States to evaluate methods which measure hillslope length in a range of tectonic, climatic and lithologic settings (Figure 3). Each site is covered by high resolution LiDAR data and has been the subject of previous work constraining the hillslope diffusivity in addition to the tectonic and erosional setting. Each dataset was collected by the National Center for Airborne Laser Mapping (NCALM) with point densities ranging from 5.56 to 9.84 points per m^2. These data were collected with horizontal accuracies ranging from 0.06 m to 0.13 m and vertical accuracies ranging from 0.05 m to 0.35 m (for full accuracy information see Supplementary Table 1). These point clouds were each gridded to 1 m resolution DEMs following standard workflows generated by Kim *et al.* (2006). This grid resolution was selected as it was the highest resolution that the point clouds could be gridded to, ensuring no variation in results driven by grid resolution changes. Lower resolution data could not be utilized for this study, as the DrEICH algorithm used to extract the channel networks cannot be used on lower resolution data (Clubb *et al.,* 2014). For each study site detailed below, we compared L_H data generated using each of the methods detailed earlier.

Coweeta, North Carolina

The Coweeta Hydrologic Laboratory is located in the Southern Appalachian Mountains in North Carolina, USA (Figure 3(a)). The landscape is underlain by Coweeta and Otto Group metasediments (Price *et al.,* 2005) and is characterized by ridge hollow topography (Hack and Goodlett, 1960) with soils approaching 2 m thickness in hollows (Hales *et al.,* 2012). Northern Hardwood forests dominate at high elevations alongside fire intolerant species such as mountain laurel (*Kalmia latifolia*) and *Rhododendron maxima,* spread due to anthropogenic fire suppression techniques in the last 80 years (Elliott and Swank, 2008; Hales *et al.,* 2009). Precipitation in Coweeta is dominated by small convective storms with occasional high intensity storms driven by hurricanes (Swift *et al.,* 1988; Hales *et al.,* 2009, 2012), such storms drive slope failures and debris flows within the catchment (Hursh, 1941; Clark, 1987; Wieczorek *et al.,* 2000; Witt, 2005; Hales *et al.,* 2009).

The Southern Appalachians are tectonically quiescent (Oyarzun *et al.,* 1997; Faill, 1998), however, the preservation of relief leads to debate regarding whether the landscape is in steady state (Baldwin *et al.,* 2003; Matmon *et al.,* 2003; Gallen
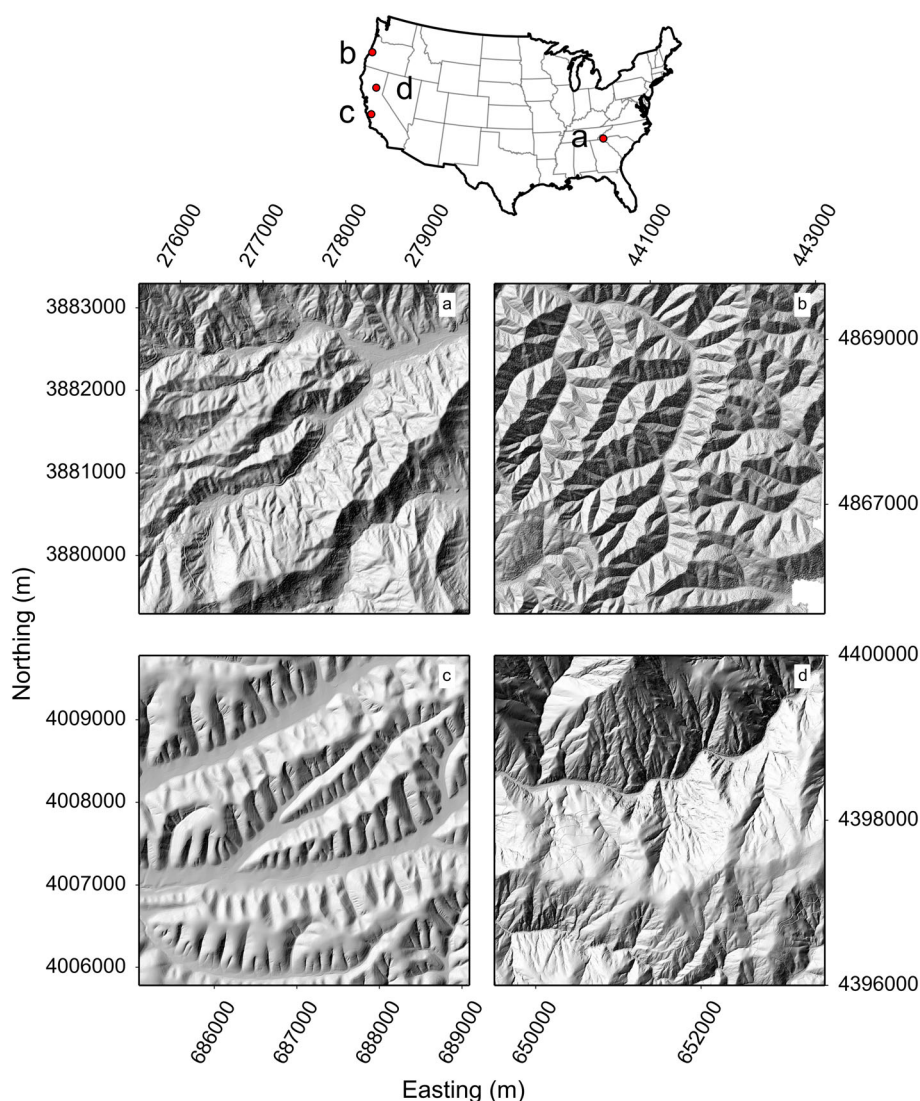

Figure 3. Shaded relief map of a representative section of each field site accompanied by a map of their locations in the continental USA. All coordinates are in UTM. (a) Coweeta, North Carolina, UTM Zone 17N. (b) Oregon Coast Range, Oregon, UTM Zone 10N. (c) Gabilan Mesa, California, UTM Zone 10N. (d) Northern Sierra Nevada, California, UTM Zone 10N. This figure is available in colour online at wileyonlinelibrary.com/journal/espl

et al., 2011, 2013). Catchment average erosion rates for the southern Appalachians have been measured from cosmogenic radionuclides at between 0.023 and 0.031 mm yr^{-1} (Matmon *et al.,* 2003) and a pilot study exploring hillslope erosion rates inside the Coweeta watershed calculated the hillslope erosion rate to be between 0.051 and 0.111 mm yr^{-1} (Hales *et al.,* 2012). These data indicate that in steeply incised terrain, such as the Coweeta Hydrologic Laboratory, the rates of hillslope erosion are governed by the rate of soil production (Hales *et al.,* 2012).

Oregon coast range, Oregon

The Oregon Coast Range in Oregon, USA (Figure 3(b)) is a humid, forested landscape with regularly spaced and heavily incised valleys (Roering *et al.,* 1999). Soils in the area range in thickness from 0.4 m on hilltops to 2 m in unchanneled valleys (Roering *et al.,* 2007), identified as common debris flow source areas (Dietrich and Dunne, 1978; Montgomery *et al.,* 2000; Heimsath *et al.,* 2001). The study area is predominantly underlain by Eocene sedimentary rocks of the Tyee Formation (Baldwin, 1956; Snavely *et al.,* 1964). Uplift rates in the OCR have been measured at between 0.1 and 0.3 mm yr^{-1} from marine terrace data (Kelsey *et al.,* 1996) which corresponds with erosion rates measured using cosmogenic radionuclides of 0.07 to 0.15 mm yr^{-1} (Beschta, 1978; Reneau and Dietrich, 1991; Bierman *et al.,* 2001; Heimsath *et al.,* 2001). These data have been taken to suggest that the Oregon Coast Range is approximately in steady state (Reneau and Dietrich, 1991; Roering *et al.,* 1999, 2007, 2010; Montgomery, 2001; Roering, 2008).

Gabilan mesa, California

Gabilan Mesa is located within the Central Coast Ranges in California, USA (Figure 3(c)) and is characterized by large linear canyons running NE to SW fed by smaller, parallel tributaries typically orientated perpendicular to the canyons (Dohrenwend, 1978, 1979; Perron *et al.,* 2008). The area has a semi-arid Mediterranean climate with most rainfall occurring between October and March (Dohrenwend, 1978) and an oak savannah ecosystem (Roering *et al.,* 2007). Soil depths are reported by Roering *et al.* (2007) to be less than 1 m thick on hilltops and thicker in unchanneled valleys. These soils overlie tectonically undeformed marine and continental sedimentary rocks of the Pancho Rico and Paso Robles Formations (Galehouse, 1967; Durham, 1974; Dohrenwend, 1978). Long-term erosion rates in the Gabilan Mesa have been estimated using surface exposure dating and the scale of valley incision into the Mesa at between 0.14 and 0.74 mm yr^{-1} (Roering *et al.,* 2007). The regularity of the valley spacing indicates that the landscape is in approximate topographic steady state (Perron *et al.,* 2009), an observation that is supported by the uniformity of the hilltop curvature across the landscape (Roering *et al.,* 2007).

Northern sierra Nevada, California

The northern Sierra Nevada of California, USA (Figure 3(d)) consists of a combination of pine and oak forest, with chaparral vegetation at lower elevations (Milodowski *et al.,* 2015) underlain by thick soils in a semi-arid climate (Yoo *et al.,* 2011; Hurst *et al.,* 2012). The topography is low relief with unevenly spaced valleys incising into a relict surface and exhibiting smooth drainage divides (Gabet *et al.,* 2015). The local geology is primarily ophiolitic, volcanic and sedimentary units of the Fiddle Creek Complex, in addition to intrusive granitoid bodies (Day and Bickford, 2004). A wide range of erosion rates have been measured in the northern Sierra Nevada, with low erosion rates found on the relict surfaces of 0.02 mm yr^{-1} and higher erosion rates of 0.25 mm yr^{-1} in canyons (Riebe *et al.,* 2000; Hurst *et al.,* 2012). However, these rates have been shown to vary through time due to accelerating tectonic uplift rates (Stock *et al.,* 2004). This results in a complex soil mantled landscape with spatially varying erosion rates driven by climatic and tectonic variations (Riebe *et al.,* 2000; Stock *et al.,* 2004; Hurst *et al.,* 2012). Hurst *et al.* (2012) and Milodowski *et al.* (2015) demonstrated that although the northern Sierra Nevada exhibits a wide range of erosion rates, due to the long response times of the channels in this landscape, the hillslopes have adjusted to local channel lowering and retain a steady topographic form. This was further demonstrated by Hurst *et al.* (2012) as this landscape plots on the steady state curve in E^* vs R^* space, whereas Hurst *et al.* (2013a) showed that transient landscapes should plot above or below the curve.

Results

Basin average measurements of hillslope length

To ensure techniques are compared against equivalent datasets, the hilltop flow routing method results are averaged over the same second-order basins used for results from slope–area and drainage density analyses. Both drainage density inversion and slope–area plots provide information about the landscape and sediment transport over millennial timescales, as both methods generalize topography through surface fitting and spatial averaging. Aspect angle is utilized in the hilltop flow routing algorithm and the surface fitting algorithm from which aspect is computed provides an effective smoothing of the topography without altering the elevation values needed for subsequent analysis. Therefore we can gain a sensible comparison between the three measures, without the influence of small-scale topographic noise on the results.

In Coweeta the basin median hillslope length from hilltop flow routing is 123 m with a median absolute deviation (MAD) of 50 m (Figure 4(a)), the median absolute deviation is a measure of statistical dispersion that is robust, i.e. performs well for probability distributions that are non-normal (Hampel *et al.,* 2011) such as our measured distributions of hillslope lengths. The large outliers seen in this dataset correspond to the large basins present in Coweeta. The slope–area data exhibit underestimation of hillslope length with a median of 28 m with a MAD of 14 m (Figure 4(b)). Few of the longer hillslopes seen in the hilltop flow routing data are reflected in the slope–area data with a strong clustering around the median value. Hillslope length values from drainage density measurements in the southern Appalachians (Figure 4(c)) reflect the smaller area covered by the Coweeta study site with a sparser distribution than seen in the other landscapes. The median lies at 58 m with a MAD of 33 m.

In the Oregon Coast Range the hilltop flow routing algorithm produces basin average hillslope lengths with a median of 89 m and a MAD of 17 m (Figure 5(a)). Results derived from slope–area measurements for this location show a skewed distribution where the majority of measurements are below 10 m, with a median value of 6 m and a MAD of 1 m (Figure 5(b)). The Oregon Coast Range drainage density derived hillslope length
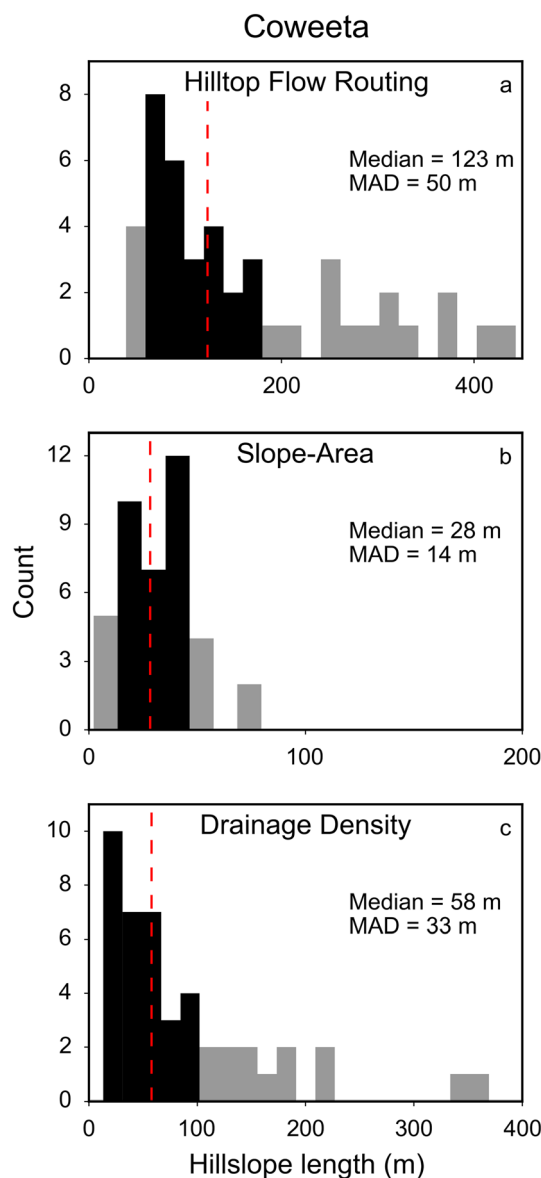
Figure 4. Histograms of basin median hillslope length for Coweeta, North Carolina calculated using: (a) hilltop flow routing; (b) slope–area analysis; and (c) inversion of drainage density. The red dashed line denotes the median and black bars indicate ±1 median absolute deviation (MAD), with the grey bars showing the remaining data. The median and MAD values for each technique are also reported. This figure is available in colour online at wileyonlinelibrary.com/journal/espl

Figure 5. Histograms of basin median hillslope length for Oregon Coast Range, Oregon calculated using: (a) hilltop flow routing; (b) slope–area analysis; and (c) inversion of drainage density. The red dashed line denotes the median and black bars indicate ±1 median absolute deviation (MAD), with the grey bars showing the remaining data. The median and MAD values for each technique are also reported. This figure is available in colour online at wileyonlinelibrary. com/journal/espl

data is normally distributed about a median of 39 m with a MAD of 10 m (Figure 5(c)).

For Gabilan Mesa the median hillslope length from hilltop flow routing is 103 m with a MAD of 26 m (Figure 6(a)). The slope–area data for Gabilan Mesa show fewer measurements overestimating hillslope length than in the other landscapes with a median value of 112 m with a MAD of 56 m (Figure 6(b)). Similar to the slope–area data, the drainage density derived measurements do not form a continuous distribution, with a lower median hillslope length of 42 m and a MAD of 14 m (Figure 6(c))

In the northern Sierra Nevada the hilltop flow routing data show a long tail extending to 400 m with a median of 104 m, and a MAD of 35 m (Figure 7(a)). Slope–area measurements for this location exhibit a skewed distribution of hillslope lengths, extending towards 2.75×10^5 m with a median value of 177 m and a MAD of 173 m (Figure 7(b)). The northern Sierra Nevada drainage density data has a similar median to the Oregon Coast Range at 33 m, but with a larger MAD of 13 m
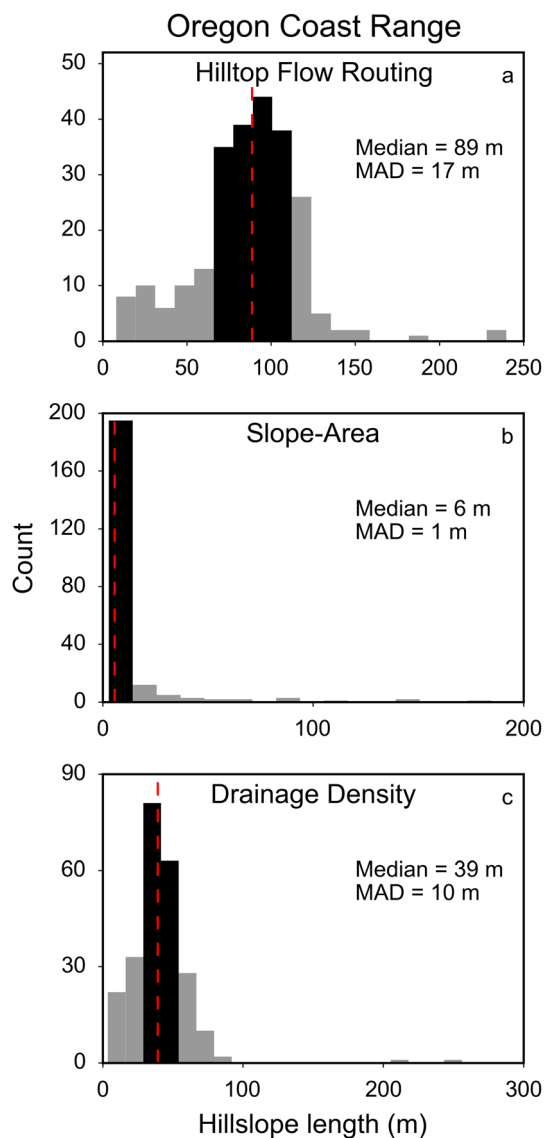
(Figure 7(c)), driven by the presence of a number of outlying basins exceeding a median hillslope length of 200 m.

Individual hillslope measurements

The Oregon Coast Range data has a median value of 98 m (Figure 8(b)) and the least variance of the four datasets, with a (MAD) of 35 m. The Coweeta and Sierra Nevada data have similar right skewed distributions but their medians differ by 100 m from 228 to 127 m, respectively (Figure 8(a), (d)). The Coweeta data shows a much larger MAD of 140 m compared with the Sierra Nevada data at 71 m. The Gabilan Mesa data is less right skewed than the Coweeta and the Sierra Nevada data with a median of 140 m and a MAD of 60 m (Figure 8(c)). The dataset shows several smaller peaks which correspond to the different length scales that can be identified in the Gabilan Mesa data.
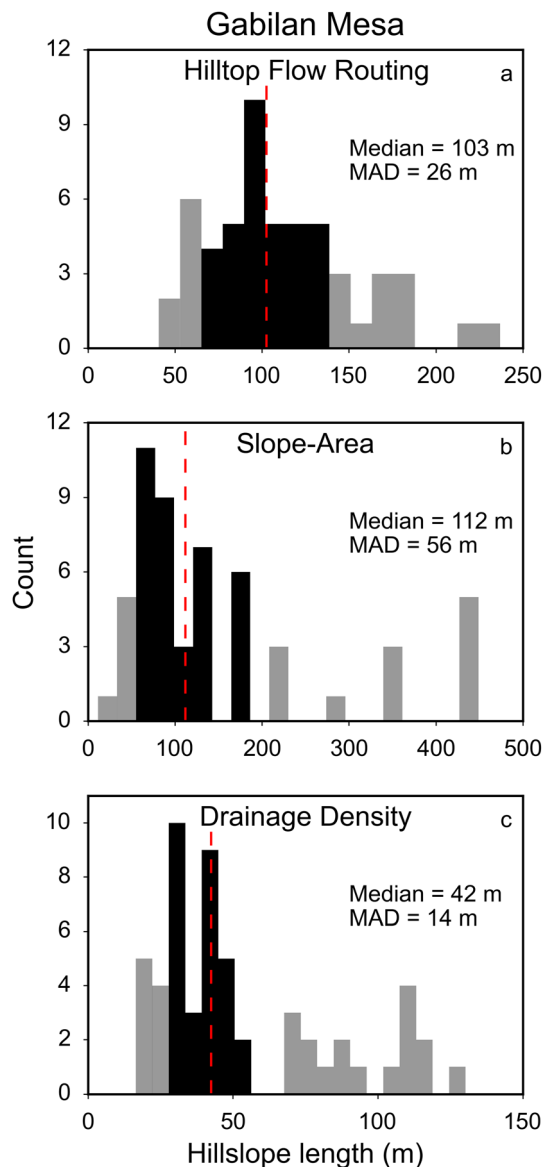
Figure 6. Histograms of basin median hillslope length for Gabilan Mesa, California calculated using: (a) hilltop flow routing; (b) slope–area analysis; and (c) inversion of drainage density. The red dashed line denotes the median and black bars indicate ±1 median absolute deviation (MAD), with the grey bars showing the remaining data. The median and MAD values for each technique are also reported. This figure is available in colour online at wileyonlinelibrary.com/journal/espl

Figure 7. Histograms of basin median hillslope length for northern Sierra Nevada, California calculated using: (a) hilltop flow routing; (b) slope–area analysis; and (c) inversion of drainage density. The red dashed line denotes the median and black bars indicate ±1 median absolute deviation (MAD), with the grey bars showing the remaining data. The median and MAD values for each technique are also reported. This figure is available in colour online at wileyonlinelibrary.com/journal/espl

Discussion

Comparison of hillslope length measurement techniques

Figure 9 presents the median and MAD hillslope length value for each technique across the four test landscapes. The slope–area derived hillslope length values for the Oregon Coast Range are distinctly different to the expected range of measurements for this locality, with most basins being underestimated by at least an order of magnitude. However the underestimation does not appear to be systematic as some of the basins have values outside the range of the expected hillslope lengths, with one basin showing a predicted median hillslope length exceeding 2×10^4 m. In both the northern Sierra Nevada and Coweeta slope–area derived datasets the llarge range within the data is driven by the large variation in basin areas found in the landscape with the largest measurements skewing the median data. As with
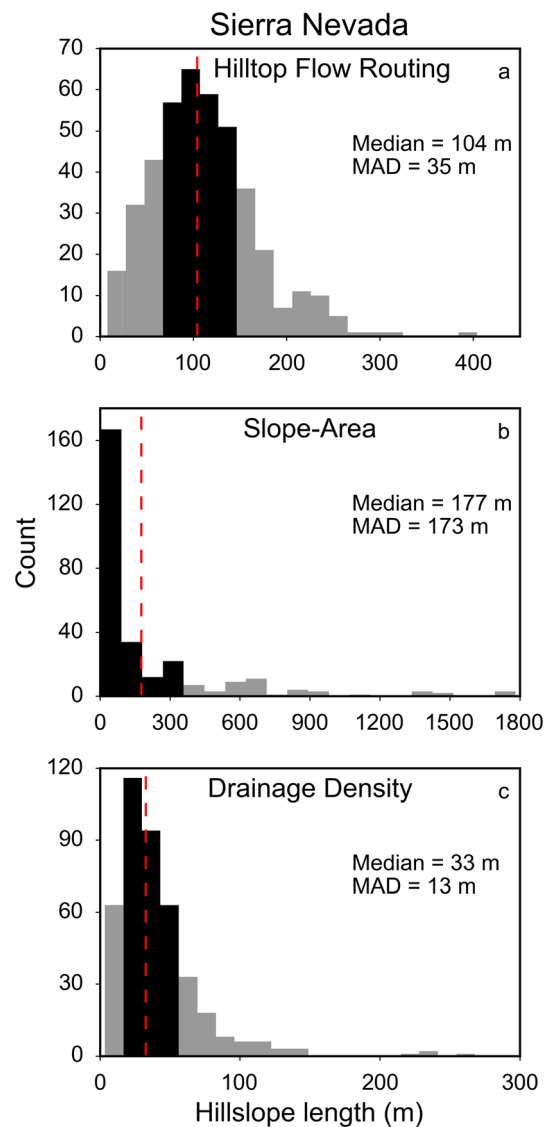
the Oregon Coast Range the modal values are at the lowest end of the distribution, showing a similar underestimation in hillslope lengths to the Oregon Coast Range data. In Gabilan Mesa the slope–area measurements appear to correlate more strongly with the hillslope length values measured from the landscape using hilltop flow routing, suggesting that the regularity of valley spacing and smoothness of the landscape in this location may facilitate more accurate slope–area measurements.

These data show the difficulty in measuring hillslope length using slope–area plots, and although in Gabilan Mesa the estimated values show good agreement with measured hillslope lengths, this pattern is not repeated in the other three landscapes. This failure of slope–area plots to predict hillslope length is not systematic, with both over- and under-estimates observed. This suggests that in steep, complex terrain with a range of processes acting upon it the slope–area technique fails to accurately capture the hillslope to valley transition point.

A fundamental problem in using slope–area plots to infer hillslope length is that the value identified by the kink in the curve is an area, not a length. This value is converted into a
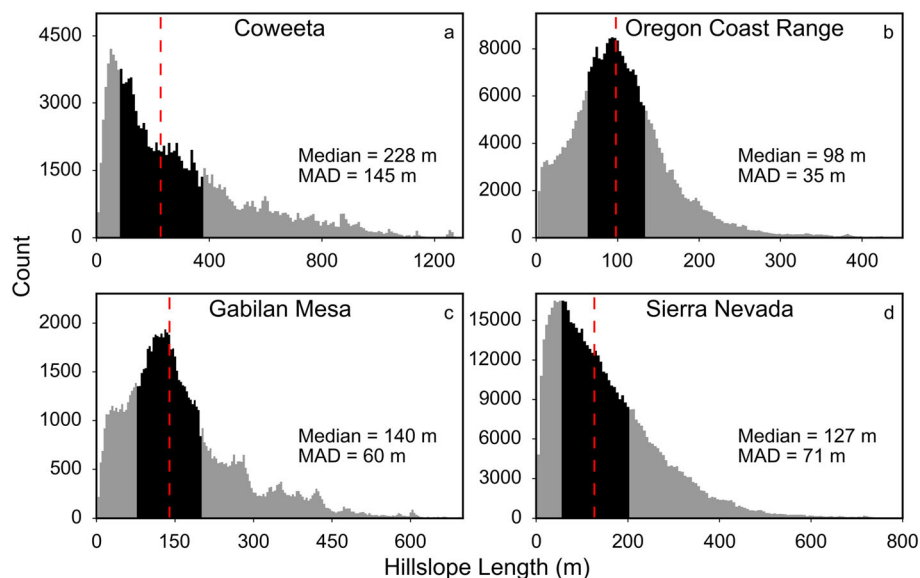
Figure 8. Histograms of hillslope length from every measured trace in each landscape. The red dashed line denotes the median and black bars indicate ±1 median absolute deviation (MAD), with the grey bars showing the remaining data. The median and MAD values for each site are also reported. (a) Coweeta, North Carolina. (b) Oregon Coast Range, Oregon. (c) Gabilan Mesa, California. (d) Northern Sierra Nevada, California. This figure is available in colour online at wileyonlinelibrary.com/journal/espl
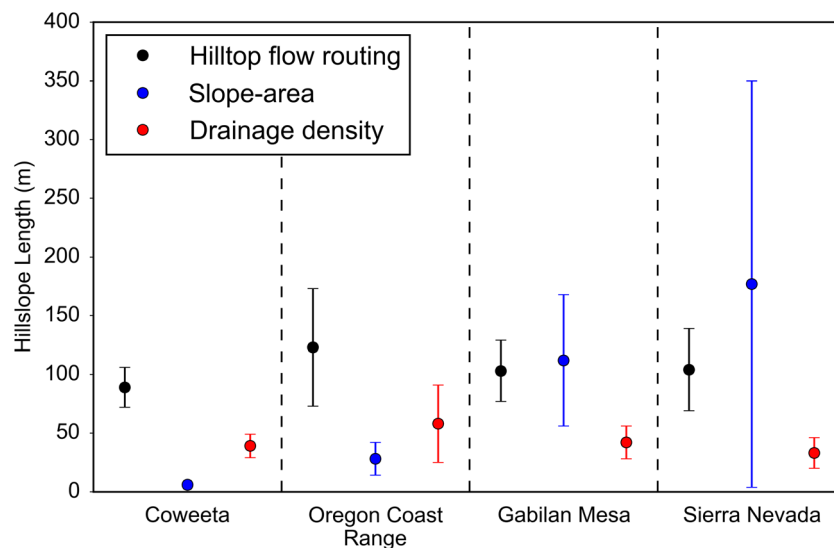

Figure 9. Comparison between the three hillslope length measurement techniques, hilltop flow routing (black), slope–area analysis (blue) and drainage density inversion (red). Error bars indicate ±1 MAD around the median value for each landscape. Black dashed lines separate measurements from different landscapes. This figure is available in colour online at wileyonlinelibrary.com/journal/espl

length by dividing the area by the unit contour width, which assumes a uniform shape of the upstream contributing area. As can be observed in nature, zero order basins are rarely this uniform, resulting in the derived length value possibly having little bearing on the actual geometry of the landscape.

In order to generate a slope–area plot following techniques described by Hancock and Evans (2006); Roering *et al.* (2007) and Tarolli and Dalla Fontana (2009), the raw slope and area data must be binned and smoothed in order to highlight the trend. This introduces free parameters and reduces the repeatability of the technique across different landscapes where different parameters may be needed to extract the inflection point (Figure 2). Although the technique can be shown to work in selected cases, it needs user supervision and modification for each individual basin it is applied to and therefore caution is required if it is to be used at the landscape scale. In this analysis the identification of an inflection point is performed automatically and in each location there are several basins where the inflection point

identified far exceeds the possible range of hillslope lengths which can be observed in the landscape.

The technique is also limited by a minimum basin size, as a sufficient number of data points are required in order to extract a signal from the data; such a limitation does not exist in the hilltop flow routing technique, which can extract hillslope lengths for individual hillslopes.

Measurements of hillslope length from drainage density systematically underestimate the value measured through hilltop flow routing in all four landscapes. Each location also has a very low variance when compared with the hilltop flow routing measurements. This highlights the inability of this method to capture the true variability in hillslope lengths which can be observed in a landscape, with the majority of basin measurements falling within a very small range of values, even in locations such as Coweeta which has a range of basin areas that scale over an order of magnitude.

The drainage density technique only requires generation of a channel network, which is routinely generated for most forms

of topographic analysis, although the value will be sensitive to the choice of method for identifying channel heads. However, the drainage destiny approach can only provide a single basin average value whereas measurement techniques using flow paths demonstrate that hillslope length can vary substantially within a basin and can therefore provide a range of values for a single basin, allowing more complex patterns of hillslope length variations to be studied across smaller spatial areas. Another benefit of using drainage density to quantify hillslope length is that it is computationally efficient and unambiguous in its implementation compared with other techniques that have many free parameters.

We observe, however, that using drainage density systematically underestimates hillslope length values when compared with flow path derived measurement techniques. Such systematic underestimation is driven by the technique's inability to capture small-scale local variations in hillslope length. This is a necessary outcome of using a basin average method and one which cannot be overcome; the urge to use smaller and smaller basins to increase the measurement resolution consequently will decrease the accuracy of the measurements as fewer streams will be included in each basin's drainage density value, making the resulting value less robust.

Spatial patterns of hillslope length from hilltop flow routing

The large range observed in both the individual hillslope and basin average hilltop flow routing data for Coweeta and the northern Sierra Nevada are driven by variations in hillslope and basin morphology. These landscapes appear transient, with incision into plateaus creating populations of steep, short hillslopes and long hillslopes running across lower gradient plateaus. The large range of basin areas, varying over an order of magnitude, produces the potential for longer hillslopes, particularly in Coweeta. When contrasting Coweeta and northern Sierra Nevada it is clear that the Coweeta dataset is not as well constrained, due to the smaller size of the area covered by the dataset, limiting the number of basins that can be studied.

The more uniform valley spacing of the Gabilan Mesa and Oregon Coast Range (Roering *et al.,* 2007; Perron *et al.,* 2009) results in a less skewed distribution of hillslope length measurements when contrasted with the other two landscapes. This is particularly apparent in Gabilan Mesa where the more rounded nature of the landscape, with less sharp transitions between hillslope and channel regimes, minimize variation in hillslope length. In the Oregon Coast Range the majority of basin average hillslope length data are within 1 MAD of the median, emphasizing the uniformity in valley spacing and basin area in this landscape. However, with these uniform landscapes a wide range of individual values are observed, highlighting the utility of the hilltop flow routing algorithm to capture topographic information at the hillslope scale.

Comparing relief with predictions from linear and nonlinear flux laws

The data from Coweeta is sparse (Figure 10(a)) with only 82 traces identified as planar across the landscape, and all of these traces occurring in lower relief sections of the landscape, yet still follows a broadly linear trend. The reduction in planar traces in this landscape may be connected to the general morphology of the Coweeta catchment, which has less regularly spaced valleys than other similar sites such as the Oregon Coast Range, presenting more opportunity for longer traces to diverge from planarity. This is exacerbated by the high incidence of landsliding reported in the study area (Hales *et al.,* 2009) which leads to increased topographic roughening.

The Oregon Coast Range data are tightly grouped along a linear trend (Figure 10(b)), showing a broad range of L_H and R values which correspond to observations of the range of valley spacing and relief made in this location (Roering *et al.,* 1999). These data highlight that the planar trace filtering method is not biasing the sampling towards certain spatial locations or topographic patterns and that the trends of L_H and relief reflect the study area as a whole.

The Gabilan Mesa is a smaller geographic area than the other three sites and correspondingly has fewer data points than the Oregon and Sierra Nevada data. However, as with the Oregon
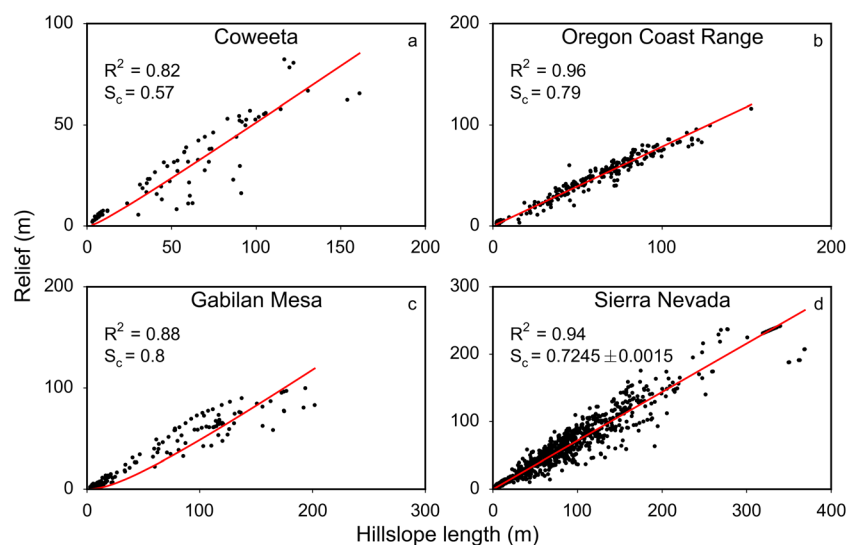

Figure 10. Scatter plots of the relationship between hillslope length and relief for each landscape. Each data point corresponds to a single hillslope trace. Red lines reflect Equation 8 fitted to the data using parameters in Supplementary Table 4. The best fit critical slope value and corresponding R^2 value are also reported. (a) Coweeta, North Carolina. (b) Oregon Coast Range, Oregon. (c) Gabilan Mesa, California. (d) Northern Sierra Nevada, California. The critical slope for this location is computed using a range of erosion rates, producing a maximum and minimum critical gradient for this landscape which differ by 0.003. As these two best fit lines are visually indistinguishable, only the line generated using the upper erosion rate bound is displayed. This figure is available in colour online at wileyonlinelibrary.com/journal/espl

Coast Range data, a broad range of values have been sampled, highlighting the ability of this technique to operate across a range of landscape morphologies, and again the data shows a linear trend. However, at longer L_H, R values stop increasing, reaching an apparent limit at approximately 100 m (Figure 10(c)) suggesting that in the highly diffusive landscape relief greater than this threshold cannot be sustained.

In the northern Sierra Nevada (Figure 10(d)) the data follows a similar pattern to the Oregon Coast Range, although there is more scatter and a larger range of values. This increased scatter is indicative of the wider range of topography in the northern Sierra Nevada, as this data captures hillslope traces from the rapidly incising canyons and from the more slowly eroding plateaus. Being able to identify a linear trend in such variable data, with no need for special processing highlights the robustness and fundamental character of the L_H–R relationship and its ability to predict nonlinear sediment flux.

In both the Oregon Coast Range and the northern Sierra Nevada the data at low R and low L_H values show much less variance than the remainder of the data for each site. These data points correspond to hilltops located close to the outlet of catchments, which produce very short, planar traces with little variation in the measurements. Such a lack of variation has no impact on the overall patterns in the data and as such there is no requirement to exclude these points from further analysis.

This independent evidence for nonlinear flux is not dependent on collecting erosion rate data or an erosion gradient in a landscape, as is required when analyzing $E^* R^*$ data to constrain sediment flux laws (Roering *et al.,* 2007; Hurst *et al.,* 2012). This technique provides clear evidence for the sediment flux law operating on a range of landscapes and highlights that hillslopes are able to record information about the sediment transport process which can be quantified through topographic analysis.

Through the use of published parameters K, ρ_r, ρ_s and E (see Supplementary Table 4 for parameter values) Equation (8) can be fitted to each dataset to test how well this model explains real topography. The best fit of Equation (8) to the Coweeta dataset uses $S_c = 0.57$ ($R^2 = 0.82$). This predicted critical gradient is low and suggests that processes other than the creep-like sediment transport described by Equation (1) may be operating in Coweeta that limit relief of hillslope traces. We can say with confidence, however, due to this strong relief limit, that a linear sediment flux law such as that described by Equation (3) is not appropriate in this landscape.

In the Oregon Coast Range the predicted S_c is 0.79 with $R^2 = 0.96$, this gradient falls below the value reported by Roering *et al.* (2007) of 1.2 ± 0.1, however, it is within published ranges of critical slope values for similar landscapes (Hurst *et al.,* 2012). This predicted critical gradient is lower than a large proportion of the hillslopes in the Oregon Coast Range, and this discrepancy may indicate that Equation (8) does not fully capture the range of sediment transport processes occurring in the Oregon Coast Range.

A similar critical gradient of 0.7245 ± 0.0015 ($R^2 = 0.94$) is predicted for the northern Sierra Nevada, with the small error bounds generated by performing the fit using the erosion rate from the rapidly eroding canyon and from the more slowly eroding plateau, which is similar to the predicted value of 0.8 from Hurst *et al.* (2012) which was estimated using $E^* R^*$ data. The estimate of Hurst *et al.* (2012) requires averaging relief and ridgetop curvature along ridgetop segments, which are then themselves binned and averaged. In addition the $E^* R^*$ technique requires a range of erosion rates to constrain the value. The predicted critical gradient for the Gabilan Mesa is equal to the lower bounds of the previously published value of 1.2 ± 0.4 (Roering *et al.,* 1999) at 0.8 with $R^2 = 0.88$. However, due to the highly diffusive nature of Gabilan Mesa the

model does not explain the L_H–R relationship as well as in other landscapes.

However, the published values of erosion rate and diffusivity are less well constrained for Gabilan Mesa than in the other landscapes (Roering *et al.,* 2007). If the diffusivity value is reduced toward the lower bound of the published range, or the erosion rate is increased toward the upper bound, this fit considerably improves, suggesting that these values may have been over- or under- estimated, respectively.

A limitation of estimating the critical gradient for a landscape using a best fit relationship is that approximately 50% of hillslopes in the landscape will have a gradient in excess of this best fit value. This can explain the discrepancy between critical gradients predicted in this study and those of Roering *et al.* (1999) which were generated by estimating the erosion rate for planar hillslopes from their morphology, and identifying the values of K and S_c which minimized the deviation from the landscape average erosion rate.

A landscape can be expected to exhibit a probability density of critical gradients, controlled by local scale variations in soil, vegetation and topographic properties (Hales *et al.,* 2009). The best fit S_c value generated using LH–R data is an averaged S_c value, representative of an average hillslope in the landscape, whereas the technique of Roering *et al.* (1999) may better constrain an upper bound for a landscape critical gradient.

Conclusions

We implement a technique to measure the length of individual hillslopes from digital topography, modelling flow as a point source travelling through DEM cells from hilltop to channel. Through the implementation of this technique two previous methods used to generate basin average hillslope lengths are evaluated. Inverting drainage density produces normally distributed hillslope lengths which systematically underestimate the true lengths of hillslopes found in a landscape. Analyzing slope–area plots for their inflection point in order to extract a characteristic hillslope length is found to be very sensitive to catchment morphology and user defined parameters, producing large amounts of uncertainty in their accuracy.

Hilltop flow routing produces robust results across a range of landscape morphologies, coping with erosional gradients, vegetation changes and differing tectonic regimes. The technique allows for exploration of the variability of hillslope length within a landscape for the first time. By using this flow path method the relationship between relief and hillslope length is explored, providing evidence of nonlinear sediment transport processes in four test landscapes. It is also shown that the critical gradient used in the nonlinear flux model can be constrained. In three of the four test landscapes the predicted critical gradient is shown to be lower than previously published, suggesting that this value may represent the average of a population of critical gradients across a landscape, highlighting the heterogeneity of landscape properties which can be found in steady state landscapes.

Author Contributions

SWDG developed the data analysis and visualization code and performed the data analysis. SWDG, SMM and MDH wrote the topographic analysis code. SWDG wrote the manuscript with contributions from SMM and MDH.

References

Abrahams AD, Ponczynski JJ. 1984. Drainage density in relation to precipitation intensity in the USA. *Journal of Hydrology* **75**: 383–388. DOI:10.1016/0022-1694(84)90061-1.

Ahnert F. 1970. A comparison of theoretical slope models with slopes in the field. *Zeitschrift für Geomorphologie* **9**: 88–101.

Ahnert F. 1987. Approaches to dynamic equilibrium in theoretical simulations of slope development. *Earth Surface Processes and Landforms* **12**: 3–15. DOI:10.1002/esp.3290120103.

Anderson RS. 1994. Evolution of the Santa Cruz Mountains, California, through tectonic growth and geomorphic decay. *Journal of Geophysical Research, Solid Earth* **99**: 20161–20179. DOI:10.1029/94JB00713.

Anderson RS. 2002. Modeling the tor-dotted crests, bedrock edges, and parabolic profiles of high alpine surfaces of the Wind River Range, Wyoming. *Geomorphology* **46**: 35–58. DOI:10.1016/S0169-555X(02)00053-3.

Andrews DJ, Bucknam RC. 1987. Fitting degradation of shoreline scarps by a nonlinear diffusion model. *Journal of Geophysical Research, Solid Earth* **92**: 12857–12867. DOI:10.1029/JB092iB12p12857.

Armstrong AC. 1980. Simulated slope development sequences in a three-dimensional context. *Earth Surface Processes* **5**: 265–270. DOI:10.1002/esp.3760050304.

Armstrong AC. 1987. Slopes, boundary conditions, and the development of convexo-concave forms – some numerical experiments. *Earth Surface Processes and Landforms* **12**: 17–30. DOI:10.1002/esp.3290120104.

Arrowsmith JR, Pollard DD, Rhodes DD. 1996. Hillslope development in areas of active tectonics. *Journal of Geophysical Research, Solid Earth* **101**: 6255–6275. DOI:10.1029/95JB02583.

Baldwin EM. 1956. Geologic map of the lower Siuslaw River area, Oregon. United States Geological Survey Oil and Gas Invest. Map OM-186.

Baldwin JA, Whipple KX, Tucker GE. 2003. Implications of the shear stress river incision model for the timescale of postorogenic decay of topography. *Journal of Geophysical Research, Solid Earth* **108**: 2158. DOI:10.1029/2001JB000550.

Beschta RL. 1978. Long-term patterns of sediment production following road construction and logging in the Oregon Coast Range. *Water Resources Research* **14**: 1011–1016. DOI:10.1029/WR014i006p01011.

Bierman P, Clapp E, Nichols K, Gillespie A, Caffee MW. 2001. Using cosmogenic nuclide measurements in sediments to understand background rates of erosion and sediment transport. In *Landscape Erosion and Evolution Modeling*, Harmon RS and III WWD (eds). Springer: USA; 89–115. [online] Available from: http://link.springer.com/chapter/10.1007/978-1-4615-0575-4_5 (Accessed 16 January 2015).

Booth AM, Roering JJ, Rempel AW. 2013. Topographic signatures and a general transport law for deep-seated landslides in a landscape evolution model. *Journal of Geophysical Research, Earth Surface* **118**: 603–624. DOI:10.1002/jgrf.20051.

Braun J, Heimsath AM, Chappell J. 2001. Sediment transport mechanisms on soil-mantled hillslopes. *Geology* **29**: 683–686. DOI:10.1130/0091-7613(2001)029<0683:STMOSM>2.0.CO;2.

Braun J, Willett SD. 2013. A very efficient O(n), implicit and parallel method to solve the stream power equation governing fluvial incision

and landscape evolution. *Geomorphology* **180–181**: 170–179. DOI:10.1016/j.geomorph.2012.10.008.

Burbank DW, Leland J, Fielding E, Anderson RS, Brozovic N, Reid MR, Duncan C. 1996. Bedrock incision, rock uplift and threshold hillslopes in the northwestern Himalayas. *Nature* **379**: 505–510. DOI:10.1038/379505a0.

Burke BC, Heimsath AM, White AF. 2007. Coupling chemical weathering with soil production across soil-mantled landscapes. *Earth Surface Processes and Landforms* **32**: 853–873. DOI:10.1002/esp.1443.

Carson MA, Kirkby MJ. 1972. *Hillslope Form and Process.* Cambridge University Press: Cambridge.

Chorley RJ. 1957. Climate and morphometry. *The Journal of Geology* **65**: 628–638.

Clark GM. 1987. Debris slide and debris flow historical events in the Appalachians south of the glacial border. *Reviews in Engineering Geology* **7**: 125–138. DOI:10.1130/REG7-p125.

Clubb FJ, Mudd SM, Milodowski DT, Hurst MD, Slater LJ. 2014. Objective extraction of channel heads from high-resolution topographic data. *Water Resources Research* **50**: 4283–4304. DOI:10.1002/2013WR015167.

Cohen S, Willgoose G, Hancock G. 2009. The mARM spatially distributed soil evolution model: a computationally efficient modeling framework and analysis of hillslope soil surface organization. *Journal of Geophysical Research, Earth Surface* **114**: F03001. DOI:10.1029/2008JF001214.

Cohen S, Willgoose G, Hancock G. 2010. The mARM3D spatially distributed soil evolution model: three-dimensional model framework and analysis of hillslope and landform responses. *Journal of Geophysical Research, Earth Surface* **115**: F04013. DOI:10.1029/2009JF001536.

Costa-Cabral MC, Burges SJ. 1994. Digital elevation model networks (DEMON): a model of flow over hillslopes for computation of contributing and dispersal areas. *Water Resources Research* **30**: 1681–1692. DOI:10.1029/93WR03512.

Culling WEH. 1960. Analytical theory of erosion. *The Journal of Geology* **68**: 336–344.

Day HW, Bickford ME. 2004. Tectonic setting of the Jurassic Smartville and Slate Creek complexes, northern Sierra Nevada, California. *Geological Society of America Bulletin* **116**: 1515–1528. DOI:10.1130/B25416.1.

DiBiase RA, Heimsath AM, Whipple KX. 2012. Hillslope response to tectonic forcing in threshold landscapes. *Earth Surface Processes and Landforms* **37**: 855–865. DOI:10.1002/esp.3205.

Dietrich WE, Bellugi DG, Sklar LS, Stock JD, Heimsath AM, Roering JJ. 2003. Geomorphic transport laws for predicting landscape form and dynamics. In *Prediction in Geomorphology*, Wilcock PR and Iverson RM (eds). American Geophysical Union: Washington, D.C.; 103–132.

Dietrich WE, Dunne T. 1978. Sediment budget for a small catchment in mountainous terrain. *Z. Geomorphology Supplement* **29**: 191–206.

Dixon JL, Heimsath AM, Kaste J, Amundson R. 2009. Climate-driven processes of hillslope weathering. *Geology* **37**: 975–978. DOI:10.1130/G30045A.1.

Dohrenwend JC. 1978. Systematic valley asymmetry in the central California Coast Ranges. *Geological Society of America Bulletin* **89**: 891–900. DOI:10.1130/0016-7606(1978)89<891:SVAITC>2.0.CO;2.

Dohrenwend JC. 1979. Morphologic Analysis of Gabilan Mesa by Iterative Contour-Generalization: An Improved Method of Geomorphic Cartographic Analysis. Pacific Coast Paleogeography Field Guide #4, SEPM: 83–87.

Dunne T, Malmon DV, Mudd SM. 2010. A rain splash transport equation assimilating field and laboratory measurements. *Journal of Geophysical Research, Earth Surface* **115**: F01001. DOI:10.1029/2009JF001302.

Dunne T, Zhang W, Aubry BF. 1991. Effects of rainfall, vegetation, and microtopography on infiltration and runoff. *Water Resources Research* **27**: 2271–2285. DOI:10.1029/91WR01585.

Durham DL. 1974. Geology of the southern Salinas Valley area, California. *US Geological Survey Professional Paper* **819**: 111.

Elliott KJ, Swank WT. 2008. Long-term changes in forest composition and diversity following early logging (1919–1923) and the decline

of American chestnut (Castanea dentata). *Plant Ecology* **197**: 155–172. DOI:10.1007/s11258-007-9352-3.

Faill RT. 1998. A geologic history of the north-central Appalachians; Part 3, The Alleghany Orogeny. *American Journal of Science* **298**: 131–179. DOI:10.2475/ajs.298.2.131.

Fernandes NF, Dietrich WE. 1997. Hillslope evolution by diffusive processes: the timescale for equilibrium adjustments. *Water Resources Research* **33**: 1307–1318. DOI:10.1029/97WR00534.

Foufoula-Georgiou E, Ganti V, Dietrich WE. 2010. A nonlocal theory of sediment transport on hillslopes. *Journal of Geophysical Research, Earth Surface* **115**: F00A16. DOI: 10.1029/2009JF001280

Furbish DJ. 2003. Using the dynamically coupled behavior of land-surface geometry and soil thickness in developing and testing hillslope evolution models. In *Prediction in Geomorphology*, Wilcock PR and Iverson RM (eds). American Geophysical Union: Washington, D.C.; 169–181.

Furbish DJ, Fagherazzi S. 2001. Stability of creeping soil and implications for hillslope evolution. *Water Resources Research* **37**: 2607–2618. DOI:10.1029/2001WR000239.

Furbish DJ, Hamner KK, Schmeeckle M, Borosund MN, Mudd SM. 2007. Rain splash of dry sand revealed by high-speed imaging and sticky paper splash targets. *Journal of Geophysical Research, Earth Surface* **112**: F01001. DOI:10.1029/2006JF000498.

Furbish DJ, Roering JJ. 2013. Sediment disentrainment and the concept of local versus nonlocal transport on hillslopes. *Journal of Geophysical Research, Earth Surface* **118**: 937–952. DOI:10.1002/jgrf.20071.

Gabet EJ, Mudd SM. 2010. Bedrock erosion by root fracture and tree throw: a coupled biogeomorphic model to explore the humped soil production function and the persistence of hillslope soils. *Journal of Geophysical Research, Earth Surface* **115**: F04005. DOI:10.1029/2009JF001526.

Gabet EJ, Mudd SM, Milodowski DT, Yoo K, Hurst MD, Dosseto A. 2015. Local topography and erosion rate control regolith thickness along a ridgeline in the Sierra Nevada, California. *Earth Surface Processes and Landforms* **40**: 1779–1790. DOI:10.1002/esp.3754.

Gabet EJ, Perron JT, Johnson DL. 2014. Biotic origin for Mima mounds supported by numerical modeling. *Geomorphology* **206**: 58–66. DOI:10.1016/j.geomorph.2013.09.018.

Gabet EJ, Pratt-Sitaula BA, Burbank DW. 2004. Climatic controls on hillslope angle and relief in the Himalayas. *Geology* **32**: 629–632. DOI:10.1130/G20641.1.

Gabriels D. 1999. The effect of slope length on the amount and size distribution of eroded silt loam soils: short slope laboratory experiments on interrill erosion. *Geomorphology* **28**: 169–172. DOI:10.1016/S0169-555X(98)00107-X.

Galehouse JS. 1967. Provenance and paleocurrents of the Paso Robles formation, California. *Geological Society of America Bulletin* **78**: 951–978. DOI:10.1130/0016-7606(1967)78[951:PAPOTP]2.0.CO;2.

Gallen SF, Wegmann KW, Bohnenstieh DR. 2013. Miocene rejuvenation of topographic relief in the southern Appalachians. *GSA Today* **23**: 4–10. DOI:10.1130/GSATG163A.1.

Gallen SF, Wegmann KW, Frankel KL, Hughes S, Lewis RQ, Lyons N, Paris P, Ross K, Bauer JB, Witt AC. 2011. Hillslope response to knickpoint migration in the Southern Appalachians: implications for the evolution of post-orogenic landscapes. *Earth Surface Processes and Landforms* **36**: 1254–1267. DOI:10.1002/esp.2150.

Gilbert GK. 1909. The convexity of hilltops. *The Journal of Geology* **17**: 344–350.

Guzzetti F, Ardizzone F, Cardinali M, Rossi M, Valigi D. 2009. Landslide volumes and landslide mobilization rates in Umbria, central Italy. *Earth and Planetary Science Letters* **279**: 222–229. DOI:10.1016/j.epsl.2009.01.005.

Hack JT, Goodlett JC. 1960. *Geomorphology and forest ecology of a mountain region in the central Appalachians*. US Government Printing Office Washington: DC.

Hales TC, Ford CR, Hwang T, Vose JM, Band LE. 2009. Topographic and ecologic controls on root reinforcement. *Journal of Geophysical Research, Earth Surface* **114**: F03013. DOI:10.1029/2008JF001168.

Hales TC, Roering JJ. 2007. Climatic controls on frost cracking and implications for the evolution of bedrock landscapes. *Journal of Geophysical Research, Earth Surface* **112**: F02033. DOI:10.1029/2006JF000616.

Hales TC, Scharer KM, Wooten RM. 2012. Southern Appalachian hillslope erosion rates measured by soil and detrital radiocarbon in hollows. *Geomorphology* **138**: 121–129. DOI:10.1016/j.geomorph.2011.08.030.

Hampel FR, Ronchetti EM, Rousseeuw PJ, Stahel WA. 2011. *Robust Statistics: The Approach Based on Influence Functions*. John Wiley & Sons: New York.

Hancock GR, Evans KG. 2006. Channel head location and characteristics using digital elevation models. *Earth Surface Processes and Landforms* **31**: 809–824. DOI:10.1002/esp.1285.

Heimsath AM, Dietrich WE, Nishiizumi K, Finkel RC. 2001. Stochastic processes of soil production and transport: erosion rates, topographic variation and cosmogenic nuclides in the Oregon Coast Range. *Earth Surface Processes and Landforms* **26**: 531–552. DOI:10.1002/esp.209.

Heimsath AM, Furbish DJ, Dietrich WE. 2005. The illusion of diffusion: field evidence for depth-dependent sediment transport. *Geology* **33**: 949–952. DOI:10.1130/G21868.1.

Herman F, Braun J. 2006. A parametric study of soil transport mechanisms. *Geological Society of America Special Papers* **398**: 191–200.

Hilley GE, Arrowsmith JR. 2008. Geomorphic response to uplift along the Dragon's Back pressure ridge, Carrizo Plain, California. *Geology* **36**: 367–370. DOI:10.1130/G24517A.1.

Horton RE. 1932. Drainage-basin characteristics. *Transactions, American Geophysical Union* **13**: 350. DOI:10.1029/TR013i001p00350.

Horton RE. 1945. Erosional development of streams and their drainage basins; hydrophysical approach to quantitative morphology. *Geological Society of America Bulletin* **56**: 275–370. DOI:10.1130/0016-7606(1945)56[275:EDOSAT]2.0.CO;2.

Howard AD. 1997. Badland morphology and evolution: Interpretation using a simulation model. *Earth Surface Processes and Landforms* **22**: 211–227.

Hursh CR. 1941. *The geomorphic aspects of mudflows as a type of accelerated erosion in the Southern Appalachian*. American Geophysics Union Reports and Papers: General Assembly: 253–254.

Hurst MD, Mudd SM, Walcott R, Attal M, Yoo K. 2012. Using hilltop curvature to derive the spatial distribution of erosion rates. *Journal of Geophysical Research, Earth Surface* **117**: F02017. DOI:10.1029/2011JF002057.

Hurst MD, Mudd SM, Attal M, Hilley G. 2013a. Hillslopes record the growth and decay of landscapes. *Science* **341**: 868–871. DOI:10.1126/science.1241791.

Hurst MD, Mudd SM, Yoo K, Attal M, Walcott R. 2013b. Influence of lithology on hillslope morphology and response to tectonic forcing in the northern Sierra Nevada of California. *Journal of Geophysical Research, Earth Surface* **118**: 832–851. DOI:10.1002/jgrf.20049.

Hurst MD, Ellis MA, Royse KR, Lee KA, Freeborough K. 2013c. Controls on the magnitude-frequency scaling of an inventory of secular landslides. *Earth Surface Dynamics* **1**: 67–78. DOI:10.5194/esurf-1-67-2013.

Jefferson AJ, McGee RW. 2013. Channel network extent in the context of historical land use, flow generation processes, and landscape evolution in the North Carolina Piedmont. *Earth Surface Processes and Landforms* **38**: 601–613. DOI:10.1002/esp.3308.

Julian JP, Elmore AJ, Guinn SM. 2012. Channel head locations in forested watersheds across the mid-Atlantic United States: a physiographic analysis. *Geomorphology* **177–178**: 194–203. DOI:10.1016/j.geomorph.2012.07.029.

Kelsey HM, Ticknor RL, Bockheim JG, Mitchell E. 1996. Quaternary upper plate deformation in coastal Oregon. *Geological Society of America Bulletin* **108**: 843–860. DOI:10.1130/0016-7606(1996)108<0843:QUPDIC>2.3.CO;2.

Kim H, Arrowsmith J, Crosby CJ, Jaeger-Frank E, Nandigam V, Memon A, Conner J, Baden SB, Baru C. 2006. An efficient implementation of a local binning algorithm for digital elevation model generation of LiDAR/ALSM dataset. Eos Transactions AGU 87 (52) Fall Meeting Supplement, Abstract G53C-0921.

Kinnell PIA. 2009. The influence of raindrop induced saltation on particle size distributions in sediment discharged by rain-impacted flow on planar surfaces. *Catena* **78**: 2–11. DOI:10.1016/j.catena.2009.01.008.

Klar A, Aharonov E, Kalderon-Asael B, Katz O. 2011. Analytical and observational relations between landslide volume and surface area.

Journal of Geophysical Research, Earth Surface **116**: F02001. DOI:10.1029/2009JF001604.

Koons PO. 1989. The topographic evolution of collisional mountain belts; a numerical look at the Southern Alps, New Zealand. *American Journal of Science* **289**: 1041–1069. DOI:10.2475/ajs.289.9.1041.

Korup O. 2008. Rock type leaves topographic signature in landslide-dominated mountain ranges. *Geophysical Research Letters* **35**: L11402. DOI:10.1029/2008GL034157.

Lashermes B, Foufoula-Georgiou E, Dietrich WE. 2007. Channel network extraction from high resolution topography using wavelets. *Geophysical Research Letters* **34**: L23S04. DOI:10.1029/2007GL031140.

Lea NL. 1992. An aspect driven kinematic routing algorithm. In *Overland Flow: Hydraulics and Erosion Mechanics*, Vol. **147–175**. Chapman & Hall: New York.

Liu BY, Nearing MA, Shi PJ, Jia ZW. 2000. Slope length effects on soil loss for steep slopes. *Soil Science Society of America Journal* **64**: 1759. DOI:10.2136/sssaj2000.6451759x.

Mark DM. 1984. Part 4: Mathematical, algorithmic and data structure issues: automated detection of drainage networks from digital elevation models. *Cartographica: The International Journal for Geographic Information and Geovisualization* **21**: 168–178. DOI:10.3138/10LM-4435-6310-251R.

Mathier L, Roy AG, Paré JP. 1989. The effect of slope gradient and length on the parameters of a sediment transport equation for sheetwash. *Catena* **16**: 545–558. DOI:10.1016/0341-8162(89)90041-6.

Matmon A, Bierman PR, Larsen J, Southworth S, Pavich M, Caffee M. 2003. Temporally and spatially uniform rates of erosion in the southern Appalachian Great Smoky Mountains. *Geology* **31**: 155–158. DOI:10.1130/0091-7613(2003)031<0155:TASURO>2.0.CO;2.

McKean JA, Dietrich WE, Finkel RC, Southon JR, Caffee MW. 1993. Quantification of soil production and downslope creep rates from cosmogenic 10Be accumulations on a hillslope profile. *Geology* **21**: 343–346. DOI:10.1130/0091-7613(1993)021<0343:QOSPAD>2.3.CO;2.

Milodowski DT, Mudd SM, Mitchard ET. 2015. Erosion rates as a potential bottom-up control of forest structural characteristics in the Sierra Nevada Mountains. *Ecology* **96**: 31–38.

Mitasova H, Hofierka J, Zlocha M, Iverson LR. 1996. Modelling topographic potential for erosion and deposition using GIS. *International Journal of Geographical Information Systems* **10**: 629–641. DOI:10.1080/02693799608902101.

Moglen GE, Eltahir EAB, Bras RL. 1998. On the sensitivity of drainage density to climate change. *Water Resources Research* **34**: 855–862. DOI:10.1029/97WR02709.

Montgomery DR. 2001. Slope distributions, threshold hillslopes, and steady-state topography. *American Journal of Science* **301**: 432–454. DOI:10.2475/ajs.301.4-5.432.

Montgomery DR, Brandon MT. 2002. Topographic controls on erosion rates in tectonically active mountain ranges. *Earth and Planetary Science Letters* **201**: 481–489. DOI:10.1016/S0012-821X(02)00725-2.

Montgomery DR, Dietrich WE. 1989. Source areas, drainage density, and channel initiation. *Water Resources Research* **25**: 1907–1918. DOI:10.1029/WR025i008p01907.

Montgomery DR, Dietrich WE. 1992. Channel initiation and the problem of landscape scale. *Science* **255**: 826–830.

Montgomery DR, Foufoula-Georgiou E. 1993. Channel network source representation using digital elevation models. *Water Resources Research* **29**: 3925–3934. DOI:10.1029/93WR02463.

Montgomery DR, Schmidt KM, Greenberg HM, Dietrich WE. 2000. Forest clearing and regional landsliding. *Geology* **28**: 311–314. DOI:10.1130/0091-7613(2000)28<311:FCARL>2.0.CO;2.

Moore ID, Grayson RB, Ladson AR. 1991. Digital terrain modelling: a review of hydrological, geomorphological, and biological applications. *Hydrological Processes* **5**: 3–30. DOI:10.1002/hyp.3360050103.

Mudd SM, Furbish DJ. 2004. Influence of chemical denudation on hillslope morphology. *Journal of Geophysical Research, Earth Surface* **109** F02001. DOI:10.1029/2003JF000087.

Mudd SM, Furbish DJ. 2005. Lateral migration of hillcrests in response to channel incision in soil-mantled landscapes. *Journal of Geophysical Research, Earth Surface* **110**: F04026. DOI:10.1029/2005JF000313.

Mudd SM, Furbish DJ. 2007. Responses of soil-mantled hillslopes to transient channel incision rates. *Journal of Geophysical Research, Earth Surface* **112**: F03S18. DOI:10.1029/2006JF000516.

O'Callaghan JF, Mark DM. 1984. The extraction of drainage networks from digital elevation data. *Computer Vision Graphics and Image Processing* **28**: 323–344. DOI:10.1016/S0734-189X(84)80011-0.

Oguchi T. 1997. Drainage density and relative relief in humid steep mountains with frequent slope failure. *Earth Surface Processes and Landforms* **22**: 107–120. DOI:10.1002/(SICI)1096-9837(199702)22:2<107::AID-ESP680>3.0.CO;2-U.

Orlandini S, Tarolli P, Moretti G, Dalla Fontana G. 2011. On the prediction of channel heads in a complex alpine terrain using gridded elevation data. *Water Resources Research* **47**: W02538. DOI:10.1029/2010WR009648.

Oyarzun R, Doblas M, López-Ruiz J, Cebrá JM. 1997. Opening of the central Atlantic and asymmetric mantle upwelling phenomena: implications for long-lived magmatism in western North Africa and Europe. *Geology* **25**: 727–730. DOI:10.1130/0091-7613(1997)025<0727:OOTCAA>2.3.CO;2.

Passalacqua P, Do Trung T, Foufoula-Georgiou E, Sapiro G, Dietrich WE. 2010. A geometric framework for channel network extraction from lidar: nonlinear diffusion and geodesic paths. *Journal of Geophysical Research, Earth Surface* **115**: F01002. DOI:10.1029/2009JF001254.

Pelletier JD. 2010. Minimizing the grid-resolution dependence of flow-routing algorithms for geomorphic applications. *Geomorphology* **122**: 91–98. DOI:10.1016/j.geomorph.2010.06.001.

Pelletier JD, McGuire LA, Ash JL, Engelder TM, Hill LE, Leroy KW, Orem CA, Rosenthal WS, Trees MA, Rasmussen C, Chorover J. 2011. Calibration and testing of upland hillslope evolution models in a dated landscape: Banco Bonito, New Mexico. *Journal of Geophysical Research, Earth Surface* **116** F04004. DOI:10.1029/2011JF001976.

Pelletier JD. 2013. A robust, two-parameter method for the extraction of drainage networks from high-resolution digital elevation models (DEMs): evaluation using synthetic and real-world DEMs. *Water Resources Research* **49**: 75–89. DOI:10.1029/2012WR012452.

Pelletier JD, Cline ML. 2007. Nonlinear slope-dependent sediment transport in cinder cone evolution. *Geology* **35**: 1067–1070. DOI:10.1130/G23992A.1.

Perron JT, Kirchner JW, Dietrich WE. 2008. Spectral signatures of characteristic spatial scales and nonfractal structure in landscapes. *Journal of Geophysical Research, Earth Surface* **113**: F04003. DOI:10.1029/2007JF000866.

Perron JT, Kirchner JW, Dietrich WE. 2009. Formation of evenly spaced ridges and valleys. *Nature* **460**: 502–505. DOI:10.1038/nature08174.

Pinet P, Souriau M. 1988. Continental erosion and large-scale relief. *Tectonics* **7**: 563–582. DOI:10.1029/TC007i003p00563.

Price JR, Velbel MA, Patino LC. 2005. Allanite and epidote weathering at the Coweeta Hydrologic Laboratory, western North Carolina, USA. *American Mineralogist* **90**: 101–114. DOI:10.2138/am.2005.1444.

Reneau SL, Dietrich WE. 1991. Erosion rates in the southern oregon coast range: Evidence for an equilibrium between hillslope erosion and sediment yield. *Earth Surface Processes and Landforms* **16**: 307–322. DOI:10.1002/esp.3290160405.

Reneau SL, Dietrich WE, Rubin M, Donahue DJ, Jull AJT. 1989. Analysis of hillslope erosion rates using dated colluvial deposits. *The Journal of Geology* **97**: 45–63.

Riebe CS, Kirchner JW, Finkel RC. 2003. Long-term rates of chemical weathering and physical erosion from cosmogenic nuclides and geochemical mass balance. *Geochimica et Cosmochimica Acta* **67**: 4411–4427. DOI:10.1016/S0016-7037(03)00382-X.

Riebe CS, Kirchner JW, Finkel RC. 2004. Erosional and climatic effects on long-term chemical weathering rates in granitic landscapes spanning diverse climate regimes. *Earth and Planetary Science Letters* **224**: 547–562. DOI:10.1016/j.epsl.2004.05.019.

Riebe CS, Kirchner JW, Granger DE, Finkel RC. 2000. Erosional equilibrium and disequilibrium in the Sierra Nevada, inferred from cosmogenic 26Al and 10Be in alluvial sediment. *Geology* **28**: 803–806. DOI:10.1130/0091-7613(2000)28<803:EEADIT>2.0.CO;2.

Rinaldo A, Dietrich WE, Rigon R, Vogel GK, Rodrlguez-lturbe I. 1995. Geomorphological signatures of varying climate. *Nature* **374**: 632–635. DOI:10.1038/374632a0.

Roering JJ. 2008. How well can hillslope evolution models 'explain' topography? Simulating soil transport and production with high-resolution topographic data. *Geological Society of America Bulletin* **120**: 1248–1262. DOI:10.1130/B26283.1.

Roering JJ, Almond P, Tonkin P, McKean J. 2004. Constraining climatic controls on hillslope dynamics using a coupled model for the transport of soil and tracers: application to loess-mantled hillslopes, South Island, New Zealand. *Journal of Geophysical Research, Earth Surface* **109** F01010. DOI:10.1029/2003JF000034.

Roering JJ, Kirchner JW, Dietrich WE. 1999. Evidence for nonlinear, diffusive sediment transport on hillslopes and implications for landscape morphology. *Water Resources Research* **35**: 853–870. DOI:10.1029/1998WR900090.

Roering JJ, Kirchner JW, Dietrich WE. 2001. Hillslope evolution by nonlinear, slope-dependent transport: Steady state morphology and equilibrium adjustment timescales. *Journal of Geophysical Research, Solid Earth* **106**: 16499–16513. DOI:10.1029/2001JB000323.

Roering JJ, Marshall J, Booth AM, Mort M, Jin Q. 2010. Evidence for biotic controls on topography and soil production. *Earth and Planetary Science Letters* **298**: 183–190. DOI:10.1016/j.epsl.2010.07.040.

Roering JJ, Perron JT, Kirchner JW. 2007. Functional relationships between denudation and hillslope form and relief. *Earth and Planetary Science Letters* **264**: 245–258. DOI:10.1016/j.epsl.2007.09.035.

Rosenbloom NA, Anderson RS. 1994. Hillslope and channel evolution in a marine terraced landscape, Santa Cruz, California. *Journal of Geophysical Research, Solid Earth* **99**: 14013–14029. DOI:10.1029/94JB00048.

Schumm SA. 1956. Evolution of drainage systems and slopes in badlands at Perth Amboy, New Jersey. *Geological Society of America Bulletin* **67**: 597–646. DOI:10.1130/0016-7606(1956)67[597:EODSAS]2.0.CO;2.

Schürch P, Densmore AL, Rosser NJ, Lim M, McArdell BW. 2011. Detection of surface change in complex topography using terrestrial laser scanning: application to the Illgraben debris-flow channel. *Earth Surface Processes and Landforms* **36**: 1847–1859. DOI:10.1002/esp.2206.

Shelef E, Hilley GE. 2013. Impact of flow routing on catchment area calculations, slope estimates, and numerical simulations of landscape development. *Journal of Geophysical Research, Earth Surface* **118**: 2105–2123. DOI:10.1002/jgrf.20127.

Small EE, Anderson RS, Hancock GS. 1999. Estimates of the rate of regolith production using 10Be and 26Al from an alpine hillslope. *Geomorphology* **27**: 131–150. DOI:10.1016/S0169-555X(98)00094-4.

Smart G, Aberle J, Duncan M, Walsh J. 2004. Measurement and analysis of alluvial bed roughness. *Journal of Hydraulic Research* **42**: 227–237. DOI:10.1080/00221686.2004.9728388.

Snavely PD, Jr, Wagner HC, MacLeod NS. 1964. Rhythmic-bedded eugeosynclinal deposits of the Tyee formation, Oregon Coast Range. *Kansas Geological Survey Bulletin* **169**: 461–480.

Stock GM, Anderson RS, Finkel RC. 2004. Pace of landscape evolution in the Sierra Nevada, California, revealed by cosmogenic dating of cave sediments. *Geology* **32**: 193–196. DOI:10.1130/G20197.1.

Stock J, Dietrich WE. 2003. Valley incision by debris flows: evidence of a topographic signature. *Water Resources Research* **39**: 1089. DOI:10.1029/2001WR001057.

Swift Jr LW, Cunningham GB, Douglass JE. 1988. Climatology and hydrology. In *Forest Hydrology and Ecology at Coweeta*, Swank WT and Jr DAC (eds). Springer: New York; 35–55.

Tarboton DG. 1997. A new method for the determination of flow directions and upslope areas in grid digital elevation models. *Water Resources Research* **33**: 309–319. DOI:10.1029/96WR03137.

Tarboton DG, Bras RL, Rodriguez-Iturbe I. 1991. On the extraction of channel networks from digital elevation data. *Hydrological Processes* **5**: 81–100. DOI:10.1002/hyp.3360050107.

Tarolli P. 2014. High-resolution topography for understanding earth surface processes: opportunities and challenges. *Geomorphology* **216**: 295–312. DOI:10.1016/j.geomorph.2014.03.008.

Tarolli P, Dalla Fontana G. 2009. Hillslope-to-valley transition morphology: new opportunities from high resolution DTMs. *Geomorphology* **113**: 47–56. DOI:10.1016/j.geomorph.2009.02.006.

Thompson SE, Katul GG, Porporato A. 2010. Role of microtopography in rainfall-runoff partitioning: an analysis using idealized geometry. *Water Resources Research* **46**: W07520. DOI:10.1029/2009WR008835.

Tseng C-M, Lin C-W, Dalla Fontana G, Tarolli P. 2015. The topographic signature of a major typhoon. *Earth Surface Processes and Landforms* **40**: 1129–1136. DOI:10.1002/esp.3708.

Tucker GE, Bradley DN. 2010. Trouble with diffusion: reassessing hillslope erosion laws with a particle-based model. *Journal of Geophysical Research, Earth Surface* **115**: F00A10. DOI:10.1029/2009JF001264.

Tucker GE, Bras RL. 1998. Hillslope processes, drainage density, and landscape morphology. *Water Resources Research* **34**: 2751–2764. DOI:10.1029/98WR01474.

Tucker GE, Catani F, Rinaldo A, Bras RL. 2001. Statistical analysis of drainage density from digital terrain data. *Geomorphology* **36**: 187–202. DOI:10.1016/S0169-555X(00)00056-8.

Tucker GE, Slingerland R. 1997. Drainage basin responses to climate change. *Water Resources Research* **33**: 2031–2047. DOI:10.1029/97WR00409.

Vianello A, Cavalli M, Tarolli P. 2009. LiDAR-derived slopes for headwater channel network analysis. *Catena* **76**: 97–106. DOI:10.1016/j.catena.2008.09.012.

Wieczorek GF, Morgan BA, Campbell RH. 2000. Debris-flow hazards in the Blue Ridge of central Virginia. *Environmental and Engineering Geoscience* **6**: 3–23. DOI:10.2113/gseegeosci.6.1.3.

Willgoose G, Bras RL, Rodriguez-Iturbe I. 1991. Results from a new model of river basin evolution. *Earth Surface Processes and Landforms* **16**: 237–254.

Witt AC. 2005. A brief history of debris flow occurrence in the French Broad River Watershed, western North Carolina. *NC Geographic* **13**: 58–82.

Yoo K, Amundson R, Heimsath AM, Dietrich WE. 2005. Process-based model linking pocket gopher (Thomomys bottae) activity to sediment transport and soil thickness. *Geology* **33**: 917–920. DOI:10.1130/G21831.1.

Yoo K, Amundson R, Heimsath AM, Dietrich WE, Brimhall GH. 2007. Integration of geochemical mass balance with sediment transport to calculate rates of soil chemical weathering and transport on hillslopes. *Journal of Geophysical Research, Earth Surface* **112**: F02013. DOI:10.1029/2005JF000402.

Yoo K, Weinman B, Mudd SM, Hurst M, Attal M, Maher K. 2011. Evolution of hillslope soils: the geomorphic theater and the geochemical play. *Applied Geochemistry* **26**(Supplement): S149–S153. DOI:10.1016/j.apgeochem.2011.03.054.

Supporting Information

Additional supporting information may be found in the online version of this article at the publisher's web site.